

Chapter 2: Exploring the Chemical Nature of the *N*-methyl-D-aspartate (NMDA) Receptor Pore Blockade*

2.1 Introduction to Learning and Memory

2.1.1 Long-term Potentiation and Long-term Depression

In Chapter 1 we described and recognized the importance of neuroreceptors and neurotransmitters in neurobiological functions. These proteins and chemicals are implicated in both normal and abnormal or diseased biological function. The exploration of these proteins and chemicals leads to more specific questions concerning the role of these biological structures in learning and memory function. At a biological and chemical level, how does the human brain learn? What biological processes contribute to learning and the formation and function of a memory? These are complicated questions to resolve. However, at the chemical-scale, we know that many of the neuroreceptors and neurotransmitters mentioned in Chapter 1 play a vital role in these processes.

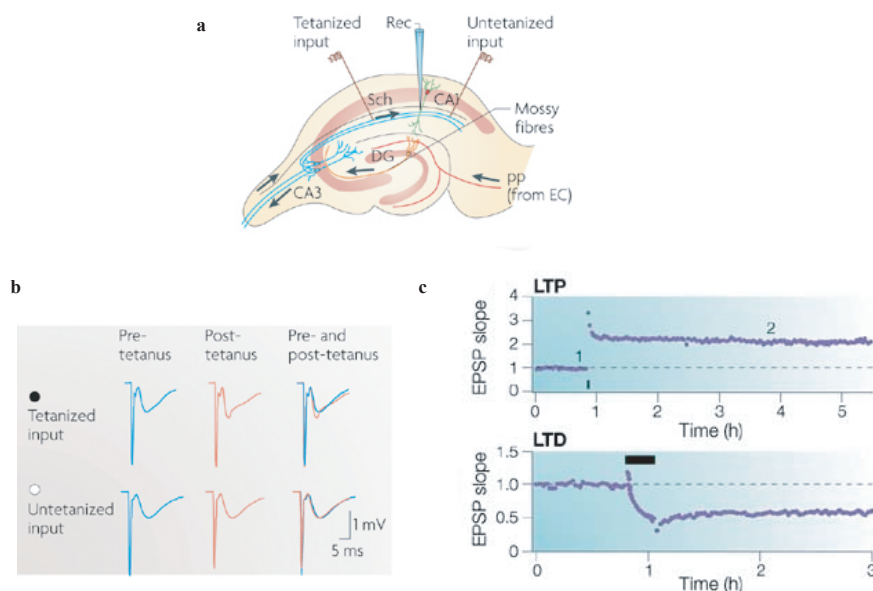


Figure 2.1 LTP and LTD. a) Hippocampal slice depicting the major excitatory neural pathways in the rat brain. b) Schematic outlining the stimulus (tetanus) applied to the hippocampal slice to induce LTP. c) LTP shown as an increase in the excitatory post-synaptic potential (EPSP) over

*Reproduced in part with permission from McMenimen, K.A., Petersson, E.J., Lesater, H.A., Dougherty, D.A. *ACS Chemical Biology* **2006**, *1*, 227–234. Copyright 2006 American Chemical Society

the baseline. LTD is demonstrated by a decrease in EPSP and is maintained for hours. Figure is adapted from (1, 2).

One approach to exploring learning and memory is to examine the manner in which neurons communicate with one another. It has been established that the central form of communication between neurons involves an electrical signal, the change to a chemical signal, and then back to an electrical signal in the next neuron. Prior study also established that for learning and memory to occur, the electrical to chemical to electrical change between neurons must take place. This process of change in the signals is referred to as synaptic plasticity. One form of synaptic plasticity occurs with the strengthening of this signal over a period of time, referred to as long-term potentiation (LTP). Its counterpart, long-term depression (LTD) is a reduction in the signal over time (Figure 2.1). LTP was discovered in the mid 1960's and has become the basis for determining how learning and memory are achieved on the molecular level (3-5).

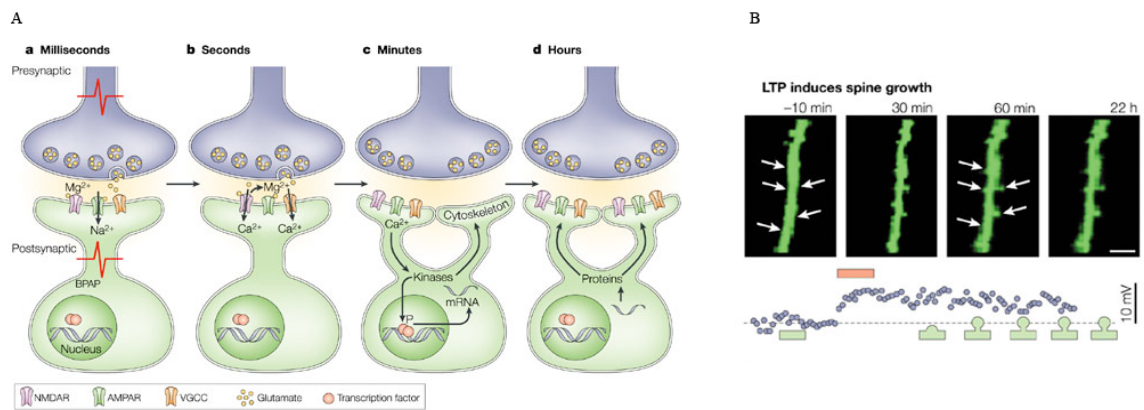


Figure 2.2 Synaptic changes after LTP induction. A) iGluRs are inserted into the synapse of cells that undergo LTP induction. Over several hours, not only is the composition of the synapse altered as more receptors are inserted into the membrane, but new synapses are formed and associated with new protein synthesis. B) LTP induces cell morphology changes as well, and over several hours new dendritic spines are created. Adapted from reference (6).

Electrophysiology performed on slices of the hippocampus show LTP induced by tetanus or large stimulus followed by recordings that remain above the baseline level recorded prior to the tetanus (Figure 2.1). In the absence of a large enough tetanus, no

LTP is recorded. The LTP counterpart, LTD results in a weakening of the synapse between cells triggered by a less intense tetanus of a longer duration (Figure 2.1c) (1, 3, 7-10). Directly extrapolating these molecular events to learning and memory formation is not possible, as many other events must take place for those large changes to occur, such as new synapse formation (Figure 2.2 A-B). However, identifying a basis for how cell-cell communication is altered over periods of time provides a starting point for determining the factors that contribute to learning and memory. Using LTP and LTD as a molecular framework will allow an exploration of the effect of changes in synaptic strength on the processes of learning and memory.

2.1.2 Synaptic Plasticity and iGluRs

On a smaller molecular scale, the molecules that contribute to some forms of LTP and LTD are LGICs(2). Although many different types of LGICs are important for communication in the central nervous system (CNS), glutamate-gated receptors (GluRs) and GABA (γ -aminobutyric acid) receptors, both ionotropic and metabotropic types, are essential for triggering synaptic transmission in learning and memory pathways (2, 11-14). The iGluRs have been a focus of our study due to their essential contribution to these intriguing and fundamental neuro-pathways and their role in diseases. The goal of our study has been to expand the nonsense suppression methodology to a new family of LGICs.

iGluRs are a superfamily of LGICs all activated by the endogenous neurotransmitter, glutamate (Glu). There are three main classes of iGluRs- the AMPA (α -amino-3-hydroxy-5-methyl-4-isoxazole-propionic acid), NMDA (N-methyl-D-aspartate), and kainate (KA) receptors- each named for their selective, synthetic agonists (Figure 2.3) (15). All of the iGluRs are tetrameric, cation-selective channels (Figure 2.4). NMDA receptors (NMDARs) are permeable to Ca^{2+} , K^{+} , and Na^{+} and AMPA and KA receptors are generally only permeable to Na^{+} and K^{+} . AMPA and NMDA receptors are directly implicated in LTP and LTD while KA receptors are indirectly associated with LTP (6, 16, 17).

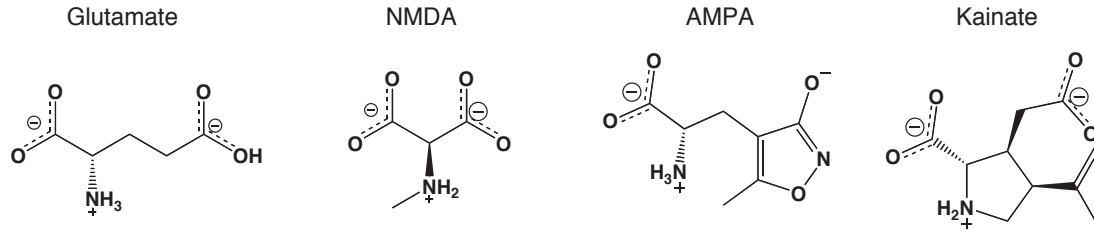


Figure 2.3 iGluR endogenous and selective agonists.

There are two general forms of synaptic plasticity, both of which rely on an alteration in AMPAR (AMPA receptor) and NMDAR in response to a stimulus (18, 19). The first form involves altering AMPARs already present at the synapse. Typically, AMPAR function is altered through a modification of an amino acid in the receptor, such as protein phosphorylation (18). Phosphorylation of serine (Ser), threonine (Thr), and tyrosine (Tyr) residues is a posttranslational modification used in many signaling pathways and other processes as a reversible method to change protein function. In the context of AMPAR and NMDARs, it is used repeatedly for targeting, trafficking, and altering protein function (20). Phosphorylation of AMPARs changes levels of postsynaptic currents contributing to LTP and LTD, but these changes in AMPAR phosphorylation are triggered by ion flow (Ca^{2+}) through NMDARs (18, 20-22).

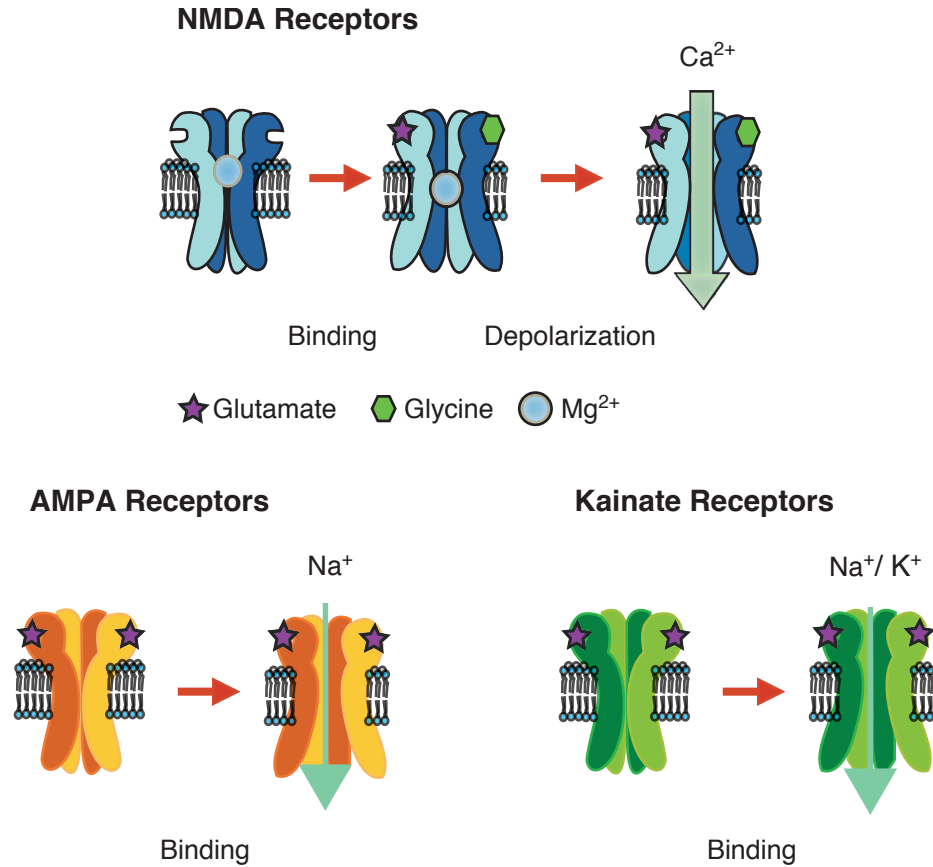


Figure 2.4 Schematic view of iGluR classes. The NMDA receptors are shown binding both glutamate and glycine. AMPA and Kainate receptors bind only glutamate. All of the iGluRs are tetrameric receptors.

The second mode of synaptic plasticity arises from alterations in protein levels, either by up or down-regulating protein production that corresponds to changes in the numbers of receptors at the synapse. Phosphorylation of AMPARs changes levels of postsynaptic currents that directly contribute to LTP and LTD. The second form of synaptic plasticity stems from changes in protein expression resulting from changes in gene regulation. These are changes in protein expression within the cell, and occur over longer time periods. Transcription of new proteins results in the formation of new synaptic connections and new proteins (may be other iGluRs or other proteins) trafficked to the membrane (23).

LTP is a complicated and very dynamic process. However, a simplified version is described to impart the importance of AMPAR and NMDARs in the process. Although both AMPARs and NMDARs are mobile and trafficked in and out of the synaptic membrane during LTP and LDP, the simplified outline begins with a few AMPARs in the synaptic membrane followed by LTP induction via newly trafficked NMDARs. AMPAR trafficking has been associated with many different proteins that associate with the synaptic membrane, such as Stargazin, a transmembrane AMPA receptor associated protein (TARP), PSD-95 (post-synaptic density protein-95), cytoskeletal proteins like actin and myosin, and several different kinases (2, 12). In general, receptors are synthesized within the cell, mobilized to the plasma membrane by exocytosis, and removed from the membrane for degradation by endocytosis. Once the receptors are at the cell surface in the membrane, they can diffuse laterally into and around the synapse (2, 12).

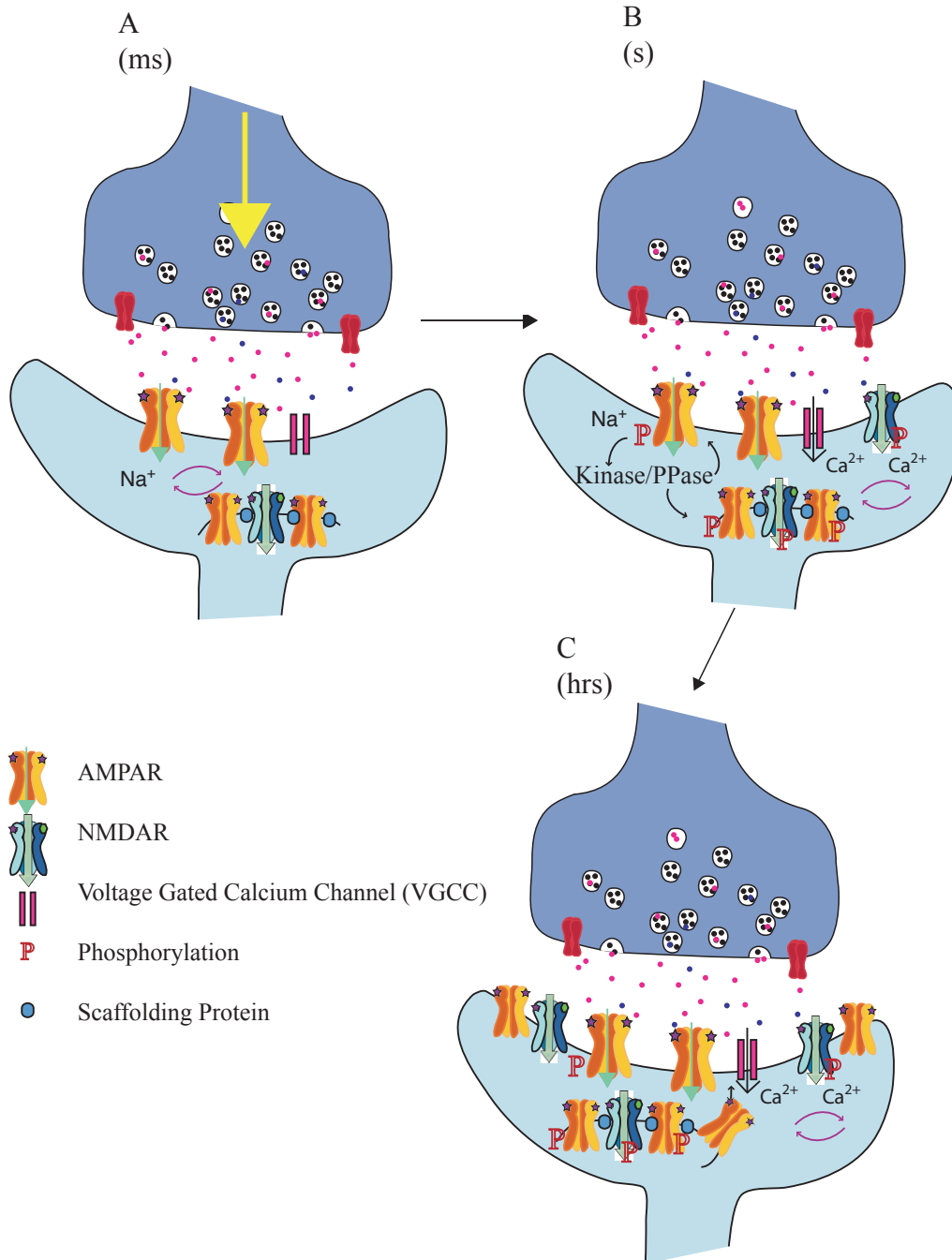


Figure 2.5 Overview of LTP. A) Basal level of control at glutamatergic synapses relies on AMPAR in the synapse. B) Sufficient membrane depolarization triggers VGCC and NMDAR activation, producing significant Ca^{2+} current into the post-synaptic cell activating kinase cascades and inducing receptor phosphorylation. C) Over longer periods of time, new receptors are trafficked into the synaptic membrane, strengthening the signal and inducing LTP.

Over short time-scales (ms) and in the absence of LTP, the release of glutamate at the synapse triggers response from AMPARs that are dynamically trafficked in and out of the synapse (13, 24). When a sufficient number of AMPARs have been activated, they cause the post-synaptic membrane to depolarize enough to open voltage-gated calcium channels (VGCCs) and NMDARs present in the membrane. The membrane depolarization is necessary to trigger NMDAR activation, but is not always sufficiently strong enough to trigger their activation (9). VGCC and NMDAR activation triggers a large flux of Ca^{2+} into the post-synaptic membrane causing activation of several kinases, such as the calcium/calmodulin-dependent protein kinase II (CaMKII) (2). These kinases can phosphorylate NMDARs, AMPARs, and other surrounding scaffolding proteins, altering the function of iGluRs (amount and type of current passing through the channel), channel trafficking and composition of the synapse (2). A change in synaptic composition is associated with an increase in AMPARs and NMDARs for LTP and a decrease in channels for LTD. These channels are typically located directly underneath the cell surface in vesicles or immediately outside of the synapse, awaiting a “signal” to send them to the synapse, which will increase the strength of the synapse by increasing the amount of current that is passed into the post-synaptic cell, inducing LTP. On a larger timescale, over hours and days, other kinases become activated (i.e., MAPK - mitogen-activated protein kinase pathway), which up-regulate gene transcription leading to new protein production (Figure 2.5). These new proteins contribute to the formation of new synapses and physically altering synapses (6).

2.1.3 The LTP Switch: NMDA Receptor Mg^{2+} Block

Although the details will be presented later in the chapter, it is important to mention one difference between AMPARs and NMDARs - the NMDAR Mg^{2+} block. It is important to remember that large Ca^{2+} currents traveling through NMDARs trigger LTP, since the currents from VGCCs are not sufficient on their own. The process of NMDAR regulation is extremely important, and one mechanism that prevents random LTP induction by NMDAR-evoked current involves a NMDAR blockade. At resting membrane potentials (no AMPAR-induced membrane depolarization) NMDARs in the cell membrane are blocked by an external Mg^{2+} ion, preventing Ca^{2+} flux into the cell

(even in the presence of Glu and Gly). Sufficient membrane depolarization (making the cell more positive, less negative relative to the outside) ejects the Mg^{2+} from the NMDAR pore, allowing Ca^{2+} flux. Overall, Glu activates AMPARs, which can depolarize the membrane enough to release NMDAR Mg^{2+} block followed by an influx of Ca^{2+} that triggers downstream signaling pathways. The function of this crucial trigger is the first target of our NMDAR studies.

LTP and LTD induction is controlled through the trafficking and physical movement of iGluRs and related proteins in and out of the synapse. These processes are controlled through a variety of very dynamic protein-protein interactions that occur between the receptors, kinases, scaffolding, and regulatory proteins (25). On a larger scale, these proteins are imaged by electron microscopy and are shown to associate in very concentrated groups (Figure 2.6A), yet are active and constantly moving depending on the signals present at the synapse. In particular, iGluRs directly associate with proteins that link to the cytoskeleton, which are involved in endo and exocytosis (Figure 2.6 B, C) (25, 26).

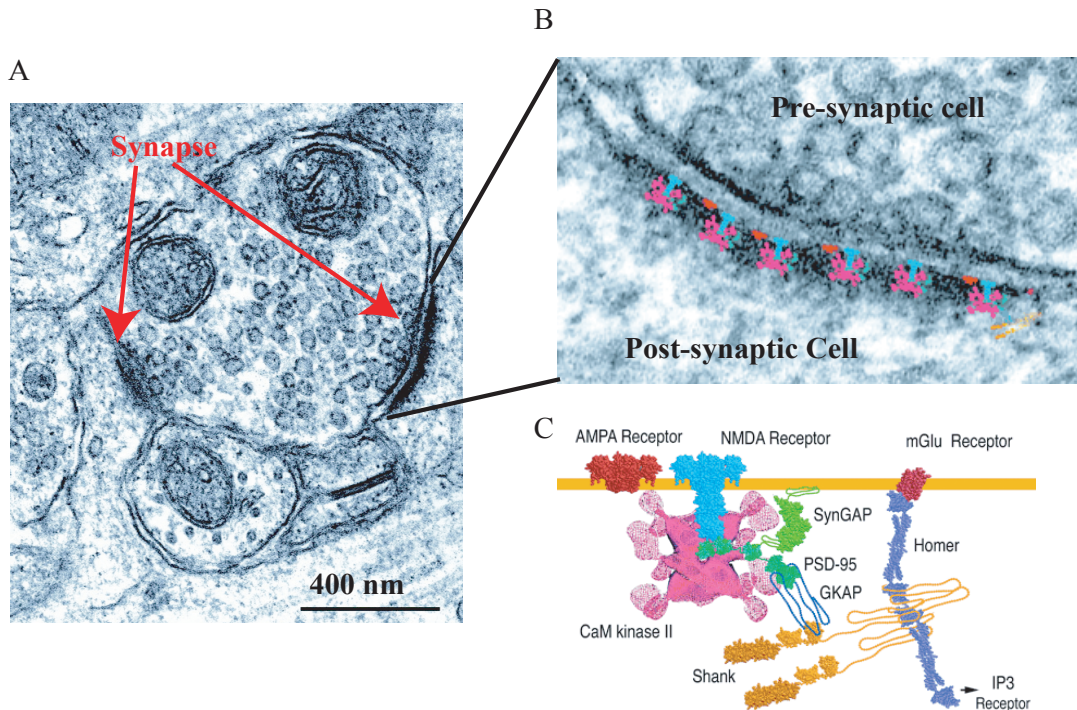


Figure 2.6 The Postsynaptic Density. A) A pre-synaptic cell associating with two dendrites forming two glutamatergic synapses. B) The synaptic interface from electron microscopy demonstrates iGluRs in the post-synaptic membrane and electron density of the surrounding associated proteins. C) Diagram representing some of the proteins that are found in electron microscopy images of the post-synaptic density. Image adapted from Kennedy, M.B.(27).

The above overview demonstrates the importance of iGluRs in synaptic plasticity and large biological processes such as learning and memory. The depicted processes generate signals between cells and explain how the signals are strengthened or weakened over time. Again, not only are the glutamate receptors important for maintaining cell-cell communication, but their dysfunction is associated with many neurodegenerative diseases. This exploration of glutamate receptors now will focus on the molecular-scale representation of these receptors.

2.1.4 Glutamate Receptor Structure and Diversity

There are several structural aspects that are conserved among all ionotropic glutamate receptors. Glutamate receptors are tetrameric, trans-membrane channels. Additionally, the tetramers are thought to associate as a dimer of dimers. Many structural aspects of

the iGluRs are different between the three families. For example, each family has a different set of subunits that can form the ion channel. There are also pre-transcriptional modifications that occur to impart diversity among the subunits, such as alternative gene splicing, and pre-translational modifications such as RNA editing. All of these modifications impart a lot of diversity among the iGluRs and create many mechanisms that allow for the regulation of functional aspects of these neuroreceptors.

AMPA receptors can be either homomeric or heteromeric channels comprised of GluR1, 2, 3, or 4 subunits, each containing approximately 850 amino acids. Typically, AMPARs are heterotetrameric channels containing GluR2 and GluR1, GluR3, or GluR4 in a symmetric “dimer of dimers” assembly (28-30). All AMPARs are activated by the binding of L-glutamate (Glu), which can bind to one site on each subunit (30). NMDARs are heterotetrameric channels composed of combinations of NR1, NR2A, 2B, 2C, and 2D subunits, each approximately 1,500 amino acids, and pass both Na⁺ and Ca²⁺. More recently, a third related gene family was discovered that codes for the NR3A and 3B subunits, which possess an inhibitory effect on receptor function (31). Kainate receptors are composed of GluR5, GluR6, GluR7, KA1, and KA2 subunits. Homotetramers form from GluR5-7 subunits while KA1 and KA2 subunits must be combined with one type of the GluR5-7 subunits (15).

All of the iGluRs gate in response to the endogenous neurotransmitter, Glu, but NMDARs also require another co-agonist for activation, which can be glycine (Gly) or D-serine (D-Ser) (15). Both of these endogenous co-agonists bind to the NR1 and NR3 (if present) subunits (Gly-binding subunits), and are present in the cytoplasm (in the CNS) at saturating concentrations required for NMDAR activation (32). Essentially, the co-agonist is always present and NMDA receptors (NR2 subunits) are activated by glutamate binding, after it is released at the synapse.

2.1.5 AMPA Receptor Diversity

Each of the GluR subunits is coded for by a separate gene and is susceptible to several post-translational modifications and RNA editing, which contributes to defining the properties of each subunit. It was established that AMPARs are always able to conduct Na⁺ current. However, this is complicated by the presence or absence of the

GluR2 subunit (present in most AMPAR channels) in the composition of the particular ion channel. AMPARs lacking the GluR2 subunit will be permeable to Na^+ , Ca^{2+} and K^+ while most GluR2-containing receptors are Ca^{2+} impermeable. The GluR2 subunit contains a neutral glutamine (residue 586) in the gene transcript, which is edited to a positively charged arginine residue in the mRNA called the Q/R site (33, 34). This is believed to prevent excitotoxicity induced by excessive Ca^{2+} flow into the cell. There is another site of RNA editing, the R/G site (arginine becomes glycine), which is only edited approximately 50% of the time in the adult brain. One additional site of editing is the flip/flop exon that is alternatively spliced. This is a 38-amino acid sequence adjacent to the final trans-membrane domain that alters the desensitization kinetics of the receptor, as a receptor containing the flip form does not desensitize (35, 36). Although there are only four GluR subunits, modifications to these subunits impart a lot of diversity that can impact the function of the ion channel. These modifications are regulated and as new receptors are transcribed, these different functionalities can be introduced into the glutamate synapse, impacting LTP and LTD.

2.1.6 NMDA Receptor Diversity

Similar to the AMPARs, the NMDARs contain great diversity as well. A single gene codes for the glycine-binding NR1 subunit. Nature cleverly uses exon splicing to produce eight variants of the NR1 subunit, which interact with different intracellular proteins, and are expressed at various developmental stages to regulate NMDAR function (37, 38). In our discussion of NMDARs we study the most common CNS splice variant, NR1a (39), which we will reference as “NR1.” The glutamate-binding subunit of the NMDAR comes in four flavors, 2A, 2B, 2C, and 2D, each one a separate gene. These subunits are expressed during different developmental periods (NR2B is up-regulated prenatally and NR2A is up-regulated postnatally) and localize in specific areas of the synapse or extra-synaptic areas of the CNS. This diversity contributes to the role iGluRs play in LTP and synaptic transmission. As will be explained, assumptions about one specific receptor will not always apply to a related receptor.

2.1.7 iGluR Subunit Topology

Relative to other neuroreceptors, a lot of structural information is known about the agonist binding domain of iGluRs (discussed in more depth in Chapter 3), however much less is known about the overall receptor structure. Limited structural data exists about the subunit topology, however, many years of biochemical experiments and data suggest that each of the iGluR subunits (independent of receptor type) contain: a large extracellular amino terminal domain (ATD), followed by an extracellular ligand-binding domain, three trans-membrane domains, and an intracellular C-terminal domain (Figure 2.7A). The size of the C-terminal domain (CTD) varies widely within the family as well as between the receptor subtypes (40). The CTD is important for maintaining interactions with scaffolding proteins in the PSD and with proteins involved in signal transduction pathways. In the EM images from Sheng and co-workers, it appears that extra density in the C-terminal region (Figure 2.7C) belongs to an AMPAR-associated protein, Stargazin (41).

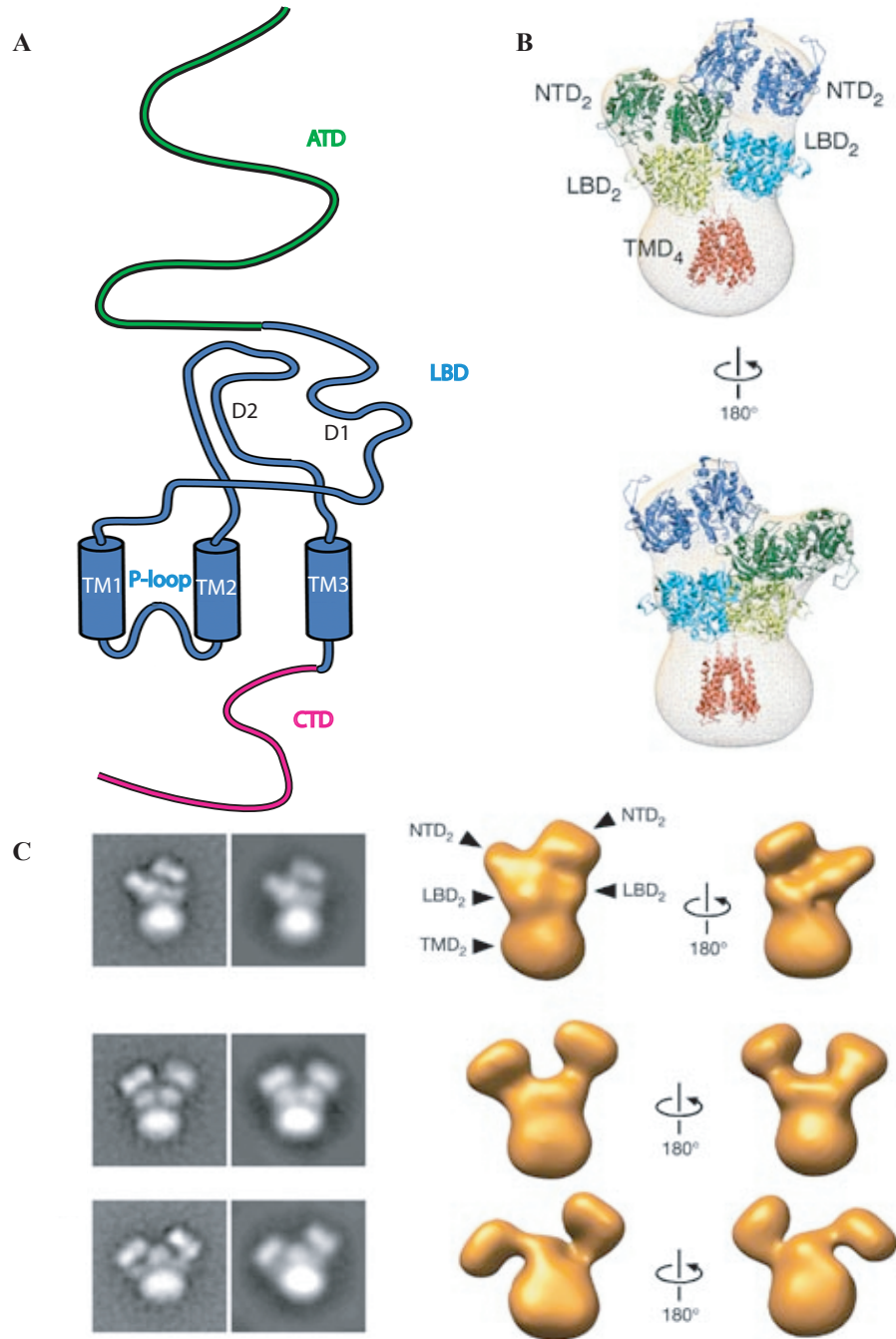


Figure 2.7 A) Topology of an individual iGluR subunit. A large cytoplasmic N-terminal domain (ATD or NTD) followed by the ligand-binding domain (LBD) composed of the D1 and D2 pieces, and three transmembrane domains with a re-entrant P-loop between TM1 and TM2. There is also an intracellular C-terminal domain (CTD) of varying length. B) Image of known crystal structures mapped onto the density map from electron microscopy of AMPARs. The crystal structures used are: extracellular domain of mGluR1 (Protein Data Bank 1EWV; dark blue

and dark green); ligand-binding domain of GluR2 (Protein Data Bank 1LBC; light blue and light green); and transmembrane segment of KcsA (Protein Data Bank 1BL8; red). Adapted from Nakagawa, T., et al. (41) C) Electron microscopy electron density maps of AMPARs showing two types of receptor structures, adapted from (41).

Much more direct structural information is available on the iGluR glutamate and glycine LBDs due to the work by Gouaux and coworkers (42-48), which we will describe in subsequent chapters. Briefly, a soluble protein containing the D1 and D2 domains (Figure 2.7A) of a NR1 or a related glutamate receptor subunit are linked together and expressed, with crystallography providing detailed structural insights into this domain of the protein. All of this work provides insight into our understanding of the function of iGluRs, particularly the LBDs. However, the trans-membrane domains in particular remain elusive.

The very limited direct structural information about the iGluRs is due to the immense difficulty in crystallizing large trans-membrane receptors. The available information suggests that the receptors are tetramers with unique subunit topology, due to a re-entrant P-loop that is reminiscent of the P-loop of the distantly related K^+ channels (49-51). The large ATD (Figure 2.7B), still un-crystallized (52), is structurally related to bacterial periplasmic binding proteins (LIV binding proteins) and the ligand-binding domain of the G-protein coupled receptor (GPCR), metabotropic glutamate receptors (mGluRs) (42, 53). Crystal structures of the bacterial amino acid-binding proteins and the ligand-binding domain of the mGluRs are modeled into electron density maps of the GluRs along with the trans-membrane domains from the K^+ channels to create a full picture of these receptors, since crystallizing the entirety of the receptors remains elusive (Figure 2.7B). This prompted our first studies of the trans-membrane region of the NMDARs and a site implicated in binding of a magnesium ion that blocks the NMDAR channel pore.

2.1.8 NMDA Receptor Mg^{2+} Block

As mentioned above, glutamate and glycine bind to the extracellular portion of the NMDAR receptor (Gly to NR1 and Glu to NR2), which initiates a conformational change

that opens the pore of the ion channel. In order for the channel to function, the Mg^{2+} ion that blocks the pore of the channel must be removed first, before Ca^{2+} can flow across the membrane (Figure 2.8). Mg^{2+} block is only alleviated by membrane depolarization (by convention, the outside of the cell has a potential of 0 mV and the inside of the cell is negative, usually -50mV to -100mV). Membrane depolarization moves the resting membrane potential toward a more positive value (towards zero). The biological implication is to make it more probable to fire an action potential. The Mg^{2+} block is one of nature's ways of preventing too much Ca^{2+} from flowing into a cell, which is directly correlated to excitotoxicity and cell death. These processes seem to be an underlying factor in the onset of some neurodegenerative diseases - just another reason why we are interested in understanding the molecular mechanisms of the Mg^{2+} block. Unfortunately, there is little structural evidence related to the Mg^{2+} binding site, which is deep within the pore of NMDARs. These initial research studies focused on the NMDA receptor and the Mg^{2+} blockade site.

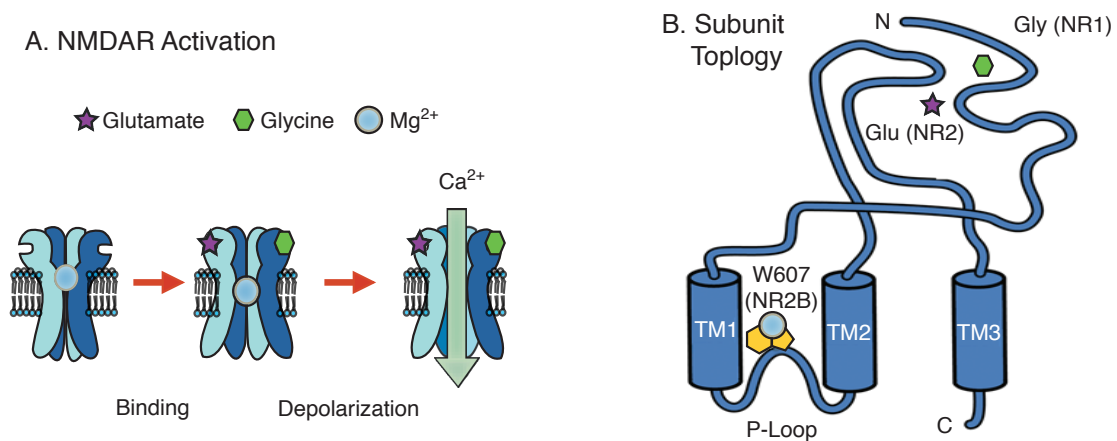


Figure 2.8 A) Schematic overview of NMDAR Mg^{2+} activation. Binding of Glu and Gly does not alleviate block, only the combination of Glu, Gly, and membrane depolarization allow Ca^{2+} flux through the receptor. B) Individual subunit topology of the NMDAR. Mg^{2+} is proposed to bind in the trans-membrane region of the pore at a site on the P-loop.

This chapter will outline several experiments aimed at understanding chemical-scale interactions involved in the pore of the NMDA receptor. The first studies will examine a proposed cation- π interaction between the Mg^{2+} ion during receptor blockade

and a conserved tryptophan (Trp607) located in the NR2 subunits. We will also examine a possible inter-subunit interaction between this Trp and an arginine (Arg630) in the NR1 subunits. The second group of experiments will explore the role of the N/Q site that is located at the narrowest constriction of the ion channel pore. We will use mutagenesis to analyze the importance of several conserved asparagines (Asn615 and Asn 616) during Mg^{2+} block and block attributed to small, synthetic organic molecules (i.e., Memantine).

2.2 Results

2.2.1 Previous Studies of the NMDAR Mg^{2+} Binding Site

Early electrophysiological studies of the NMDA receptor were able to localize the site of Mg^{2+} block and provide insights into the interaction between the ion and receptor.

Studying the voltage dependence of the block led to the proposal that blockage occurs deep within the pore of the ion channel (47, 54-57). At large hyperpolarized potentials (the inside of the cell is highly negative), Mg^{2+} can be driven through the membrane. It is likely that in order for Mg^{2+} to permeate the channel it must be dehydrated. Additional evidence for this comes from the fact that divalent metal ion permeabilities correlate inversely with dehydration energies (58). Hydrated Mg^{2+} has a diameter of 0.64 nm, which is larger than the NMDAR pore (<0.6 nm) (58-60). These studies suggest that in order for Mg^{2+} to permeate the pore, it must be stripped of its solvation shell (61).

Several studies of K^+ channels demonstrate that ion conduction through a pore can “rehydrate” or solvate dehydrated ions via ion-protein interactions as the ion travels through the pore (49, 62, 63).

that only NR2B W607 was implicated in Mg^{2+} block. A significant disparity was observed with mutations replacing the Trp with the other aromatic residues, Tyr and Phe. As seen in Figure 2.9B, IC_{50} values for Mg^{2+} increased only slightly (64) when the other aromatic amino acids replaced Trp. Receptors containing aromatic amino acid mutations in the P-loop all demonstrate wild type like responses to glutamate, glycine, and pH, implying that they are otherwise unchanged. One important caveat is that receptors containing the NR2B W607Tyr or W607Phe mutations are more permeable to Mg^{2+} than the wild-type receptors, which could be due to the size differences among the amino acids or the relative cation- π binding abilities of the side chains.

The second interaction implicated in contributing to Mg^{2+} block occurs between several highly conserved asparagine residues (NR1 N616 and NR2 N615 and N616) that appear on both NR1 and NR2 subunits (thought to lie at the apex of the turn) (Figure 2.9A,C) and the metal ion. Mutagenesis of the asparagines in NR1 and NR2 to Gly, Gln, Ser, and Asp establish that they interact with the cation through an electrostatic interaction instead of just through a steric occlusion of the pore (65-67). Wollmuth *et al.* found that block was slightly attenuated, but not abolished, when Gln was mutated to Gly or Ser and did not substantially increase upon mutation to Asp (a fully charged sidechain). Additionally, their results demonstrate that residues along the P-loop are asymmetrically involved in Mg^{2+} block. Wollmuth *et al.* propose that Mg^{2+} becomes at least partially dehydrated during block and compensates for the reduced hydration shell by obtaining a six-coordinate geometry (preferred) via interactions with the NR2A asparagines (65). The asparagines replace the hydration shell around Mg^{2+} .

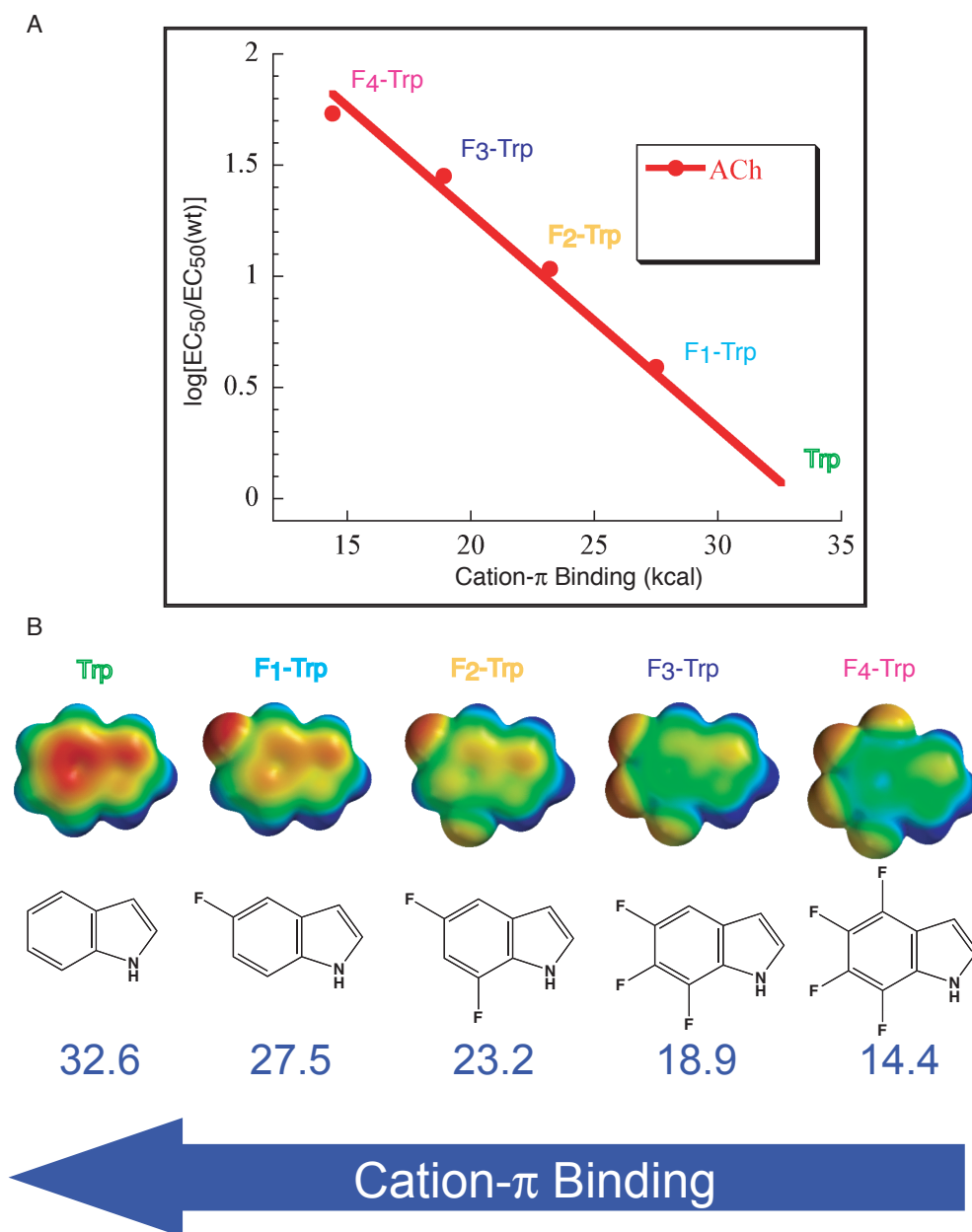


Figure 2.10 A) Cation- π plot demonstrating a linear relationship between the cation- π binding ability of the side chain aromatic amino acid and the shift in ACh EC₅₀ with each mutation. B) Electrostatic potential surfaces representing each of the fluorinated Trp side chains and the calculated cation- π binding energies

The above work established a starting point for our analysis of the NMDAR Mg²⁺ binding site. We began by focusing on the hypothesis postulated by Williams' that Mg²⁺ binds to NR2 W607 *via* a cation- π interaction. Our group had successful prior experience

incorporating fluorinated Trp residues into the ACh receptor to establish the existence of a cation- π interaction with a cationic agonist; therefore, we wanted to harness this same technique for this study (68-73). Using the fluorinated Trp series we would observe a step-wise decrease in Mg^{2+} block if a cation- π interaction contributed to blockade. This exact experiment was performed and identified a cation- π interaction between a conserved Trp (residue 149) of the muscle nicotinic acetylcholine receptor and the endogenous neurotransmitter, acetylcholine (68). The unnatural amino acid methodology is perfectly aligned for these experiments, as fluorinated Trp analogs are a precise chemical perturbation of this interaction. Fluorinated Trp is a much weaker cation- π binder than Trp, yet is almost completely isosteric, free from inflicting steric perturbations. In order to study the cation- π interaction, we sequentially replace Trp with monofluoro-, difluoro-, trifluoro-, and tetrafluoro-Trp and compared the calculated (innate) cation- π binding ability of the aromatic side chain (kcal/mol) to the EC_{50} of the agonist when the mutation is present ($\log EC_{50}$ is plotted to maintain a similar energy scale) (Figure 2.10). A similar scale was used for measuring IC_{50} as well. Initially, in the case of ACh, an exceptional correlation was observed that was later extended to explain the binding of additional agonists (68, 72).

Since we had developed a protocol for analyzing the importance of cation- π interactions, we began our investigation at the NR2B W607 site. This site was implicated in previous studies and believed to be the most important aromatic residue involved in Mg^{2+} block. It was first explored with the fluorinated Trp series. It was expected that upon incorporation of the fluorinated tryptophan residues a step-wise decrease in Mg^{2+} block would be observed if the cation- π interaction was implicated in the blockade. A linear relationship would be observed between the calculated cation- π binding energies of the fluorinated Trp side chains and the log of the measured IC_{50} from each mutation compared to wild type. These initial studies were performed in collaboration with another graduate student, E. James Petersson.

2.2.2 Wild Type NMDA Receptor Expression

Prior to unnatural amino acid mutagenesis in the NMDA receptor, a robust and reproducible expression system needed to be established for the wild type receptors.

Precedents reported in prior literature from the Williams laboratory for NMDA receptor expression in oocytes were used and constructs for NR1a and NR2B (NMDARs most sensitive to Mg^{2+} block) were obtained. These constructs were originally cloned into the pBluescript vector. However, more recent studies demonstrate that using a *Xenopus laevis* expression vector for oocytes will increase the resulting receptor yields. Therefore, both the NR1a and NR2B genes were subcloned into a vector designed for expression in oocytes, pAMV vector. pAMV is derived from pBluescript but contains an additional 5' untranslated region from the alfalfa mosaic virus that aids in binding to the ribosome (74).

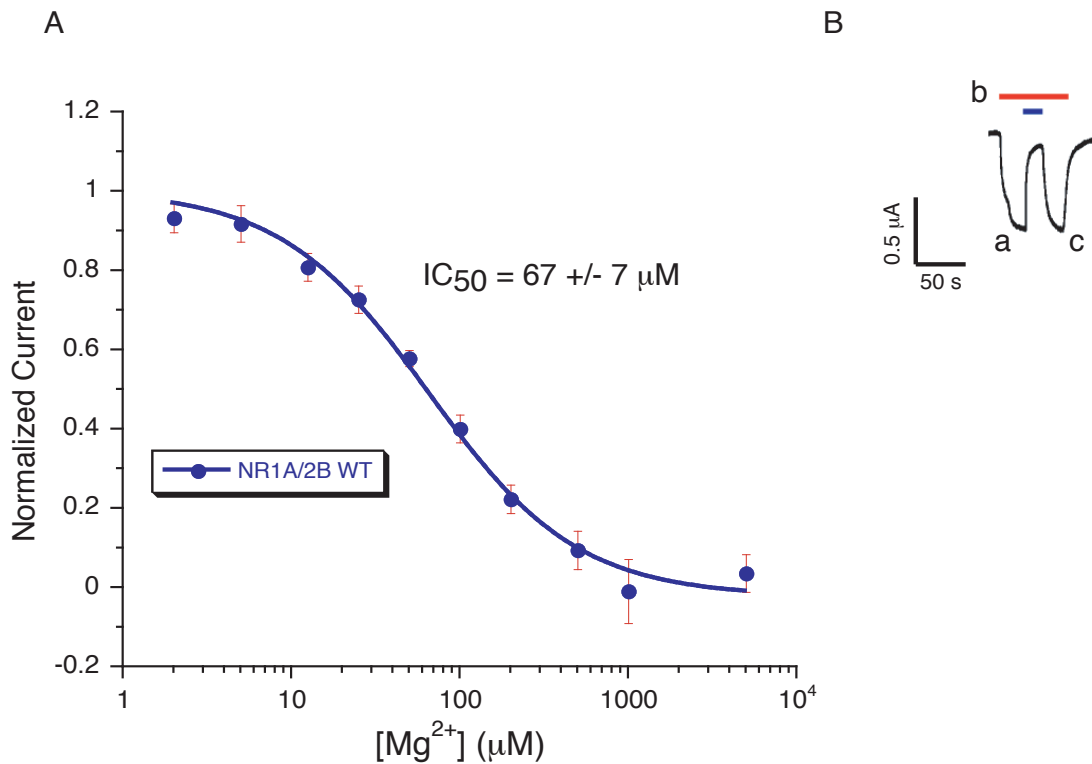


Figure 2.11 NMDA receptor Mg^{2+} block. A) Dose-response curve generated for Mg^{2+} block. B) Electrophysiology trace of wild type NR1a/NR2B receptors. Red bar = 100 μM Glu + 10 μM Gly. Blue bar = 500 μM Mg^{2+} .

Wild type NR1a/NR2B mRNA subunits were injected into *Xenopus* oocytes in a 1:1 ratio. Oocytes were incubated for a standard 2 days. A dose-response curve for Mg^{2+} block obtained of the wild type receptors (Figure 2.11A) to confirm expression.

Protocols previously described by Williams and coworkers (64) were followed. Briefly, a series of saturating doses of each agonist, 100 μM Glu and 10 μM Gly, were applied to each oocyte for a given duration of time (Figure 2.11B). EC_{50} values for Glu and Gly were determined as 1.4 μM and 0.14 μM , respectively. When obtaining EC_{50} values for Glu and Gly, a saturating dose of Gly (10 μM) or Glu (100 μM) was always applied, respectively. Concentrations much larger than the EC_{50} values are used during the experiments to ensure that full receptor activation is achieved, which is important in determining the effects of mutations on Mg^{2+} block. After the initial application of Glu and Gly (Figure 2.11B (a)), a dose of Mg^{2+} that also contains the agonists was applied (Figure 2.11B (b)), followed by a washout solution with just the agonists (Figure 2.11B (c)). This procedure reveals the receptor activation, Mg^{2+} block, and the reversibility of the blockade.

In order to generate the IC_{50} graph (Figure 2.11A), the ratio of the response (signal) in the presence and absence of Mg^{2+} versus the concentration (doses) of Mg^{2+} used to generate the IC_{50} was plotted. Previous studies have recorded the Mg^{2+} IC_{50} value at 19 μM for the wild type NR1a/2B receptor (64). Using the OpusXpress™ and the cloned constructs, the wild type NR1a/2B receptor Mg^{2+} block was recorded at 66.7 ± 7 μM (Figure 2.11A). Although this number is different from that of the Williams' lab, it is not surprising, as previously obtained EC_{50} s from acetylcholine and GABA receptors recorded on the OpusXpress™ were larger than those recorded on traditional electrophysiological rigs.

2.2.3 Control Experiments

One set of control experiments was performed due to reports of homomeric NR1a subunits forming functional channels in *Xenopus* oocytes (75, 76). In order to confirm that the responses analyzed were from properly formed heteromeric NR1a/2B receptors, the NR1a subunit mRNA was injected into oocytes without NR2 mRNA. Doses of 100 μM glutamate and 10 μM glycine were applied to the oocyte (protocol shown above). However, no current was recorded from these oocytes. This indicated that the previous experiments that produced responses to 100 μM glutamate and 10 μM glycine were in fact recording heteromeric NR1a/2B receptors.

Based on previous studies with the nicotinic acetylcholine receptor, which normally incubates for 1-2 days post mRNA injection, this incubation time was used initially. However, in order to optimize the NMDAR expression, the incubation time was altered by allowing the oocytes to incubate at 16°C for 2-4 days post mRNA injection. After 4 days of incubation post wild type NR1a/2B mRNA injection, the oocytes were unhealthy and useful data was not obtained or recorded. As a result, the optimal incubation time for wild type NR1a/2B receptors was determined to be two days. One reason why the oocytes may become unhealthy is due to the activation of Ca²⁺ activated Cl⁻ channels, which would disrupt the membrane potential of the oocyte.

After successful expression of the appropriate wild type receptors and generating reproducible results, the next step was to demonstrate the recovery of the wild type receptor phenotype using nonsense suppression to incorporate Trp at position 607 in the NR2B subunit (a “wild type recovery” experiment). Several experiments were performed to optimize unnatural amino acid incorporation into functional NMDA receptors. The experiments first began by making a TAG (stop codon) mutation at residue 607 in the NR2B gene. Wild type recovery experiments were performed by co-injecting NR1a/NR2BW607TAG mRNA (1:5 ratio) and tRNA_{CUA}-Trp. After optimizing incubation conditions again, it was concluded that 2 days produced optimal results. In order to increase expression, a “booster” injection was given to each oocyte after 24 hours of tRNA_{CUA}-Trp. The booster injection only contained tRNA_{CUA}-Trp because the limiting factor in nonsense suppression is the amount of aminoacyl tRNA that is injected into the oocyte.

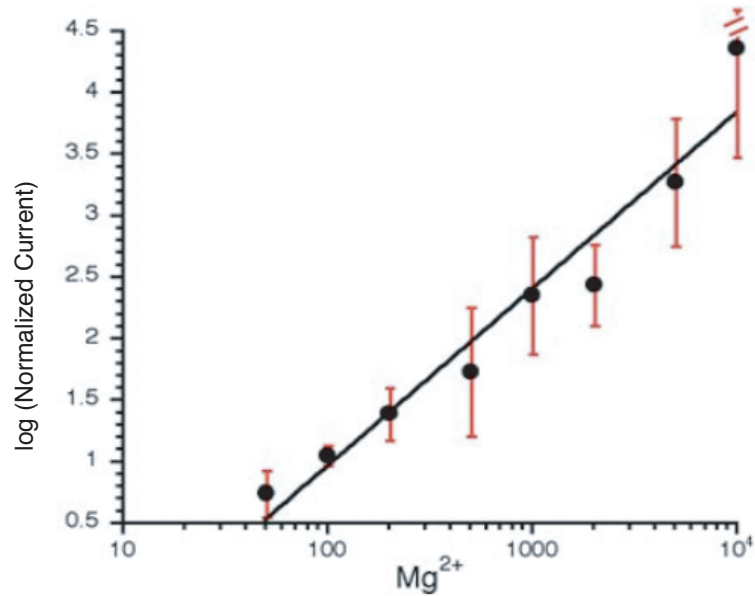


Figure 2.12 Misincorporation phenotype generated by receptors expressed from NR1a/2B607TAG mRNA co-injected with tRNA_{CUA}.

One possible complication due to the nonsense suppression method is the re-acylation of tRNA by the oocytes' endogenous aminoacyl tRNA synthetases after the unnatural amino acid is incorporated into the protein. If this occurs, it will lead to “misincorporation” of an undesired amino acid at the site of interest. In order to test the amount of misincorporation current generated, NR1a/2B607TAG mRNA was injected into oocytes without injecting the corresponding aminoacyl-tRNA. Glutamate and glycine were co-applied to these oocytes and no current was recorded. To determine if the synthetic tRNA could be used by the oocyte, as a control NR1a/2B607TAG mRNA was co-injected with an unaminoacylated tRNA_{CUA} (76 mer, biologically relevant unaminoacylated tRNA). The results produced substantial background currents. However, Mg²⁺ could not block these receptors. Instead, they were permeable to Mg²⁺ at concentrations larger than ~1000 μM. In Figure 12, the currents produced at Mg²⁺ concentrations less than 1000 μM are typical Na²⁺ currents, and the amount of current then increases as Mg²⁺ concentration increases (>1000 μM), indicative of more ion flow across the membrane. A logarithmic relationship was observed between the magnesium concentration and the NMDAR currents recorded, signifying that Mg²⁺ does not block the receptor but functions as a charge carrier (Figure 2.12) (77).

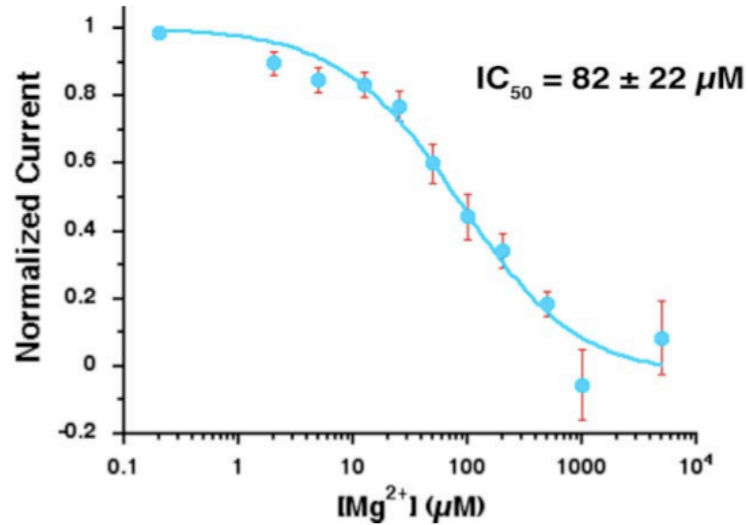


Figure 2.13 Wild type recovery experiment producing an Mg^{2+} IC_{50} of $82 \pm 22 \mu\text{M}$. NR1a/2B607TAG mRNA was co-injected with $\text{tRNA}_{\text{CUA}}\text{-Trp}$.

Williams and co-workers also found that Mg^{2+} permeates the pore for some poorly blocking mutant receptors, such as the NR2B 607Leu mutant (64). Optimization experiments conducted as part of this study demonstrated that misincorporation currents are greatly reduced when nonsense suppression experiments are performed 2 days after the initial oocyte injection. With these conditions, it was concluded that the background was sufficiently low to produce reasonable data for the unnatural amino acid experiments of this study. The first wild type recovery experiments were performed and generated a dose-response curve for Mg^{2+} block by incorporating Trp via suppression at NR2B607. The results were within error of the wild type IC_{50} value indicating successful nonsense suppression of NMDARs (Figure 2.13).

2.2.4 Incorporation of F_n -Tryptophans at NR2BW607

The above protocol was followed for expression of receptors containing F_n -Trps. NR1a/2B607TAG mRNA was co-injected with $\text{tRNA}_{\text{CUA}}\text{-F-Trp}$ to determine the importance of a cation- π interaction in Mg^{2+} block. First, it was noticed that F-Trp incorporation resulted in currents that were approximately 20% smaller than those from Trp incorporation as well as more sporadic expression levels overall, yet dose-response relationships were still generated without difficulty. As with most electrophysiological

experiments, it is important to look at traces, which are shown below for wt (wild type), Trp, and F-Trp (Figure 2.14).

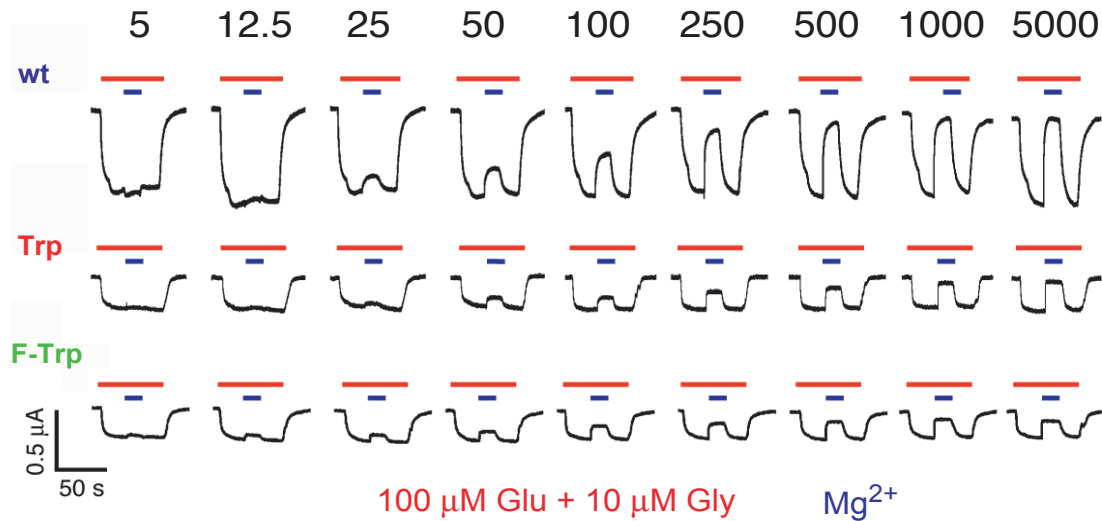


Figure 2.14 Electrophysiological traces for wt, Trp, and F-Trp incorporation in the NR1a/NR2B607 receptors. Expression levels decrease and full Mg^{2+} block is not achieved with suppressed receptors. Mg^{2+} concentrations are shown at the top in (μM).

The only observable difference between Trp and F-Trp incorporation is that full Mg^{2+} block is not observed with F-Trp incorporation. Even at high Mg^{2+} concentrations, full receptor block was not reached (Figure 2.13 and 2.14). It is likely that the small amount of “misincorporation” currents skewed the results. However, despite this data, reasonable IC_{50} values were obtained and resulted in the dose-response data comparable to wild type data.

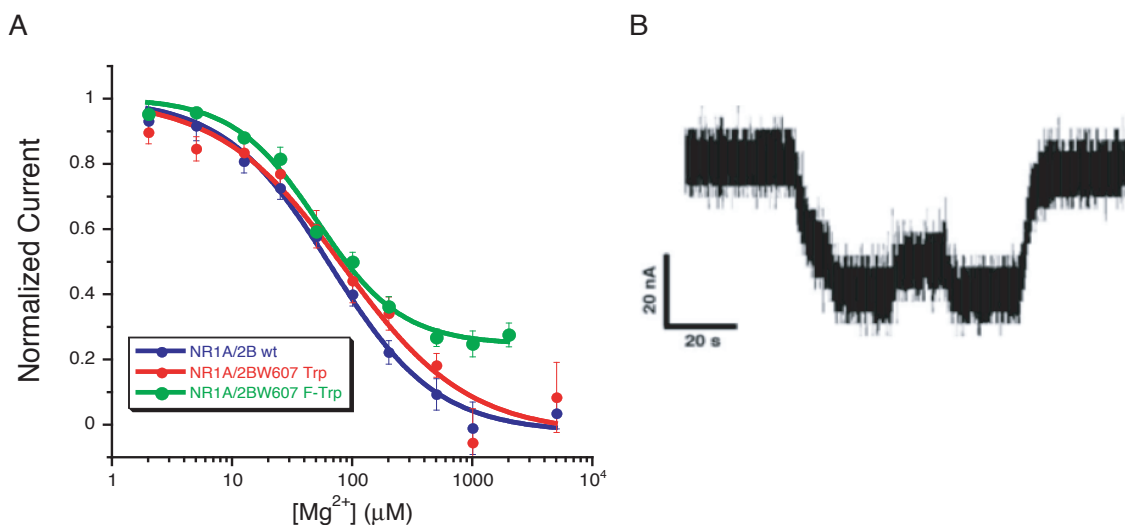


Figure 2.15 NR2BW607F Trp Data. A) IC_{50} values for Mg^{2+} block at wt, Trp, and F-Trp NMDARs. B) F_2 -Trp Electrophysiology data.

As seen above (Figure 2.15A) incorporation of F-Trp at NR2B607 did not result in a rightward (or any) shift in Mg^{2+} IC_{50} with a value of $52 \mu M$. Since no significant rightward shift was observed with NR2BW607F-Trp, it appears that a cation- π interaction is not likely to occur between W607 and the metal ion. To rule out the possibility of a cation- π interaction, F_2 -Trp was incorporated at NR2B607. Initially, small currents were recorded (Figure 2.15B), but with double injections of $tRNA_{CUA}$ - F_2 Trp increased expression was sufficient enough to determine an IC_{50} for Mg^{2+} of $52 \pm 10 \mu M$.

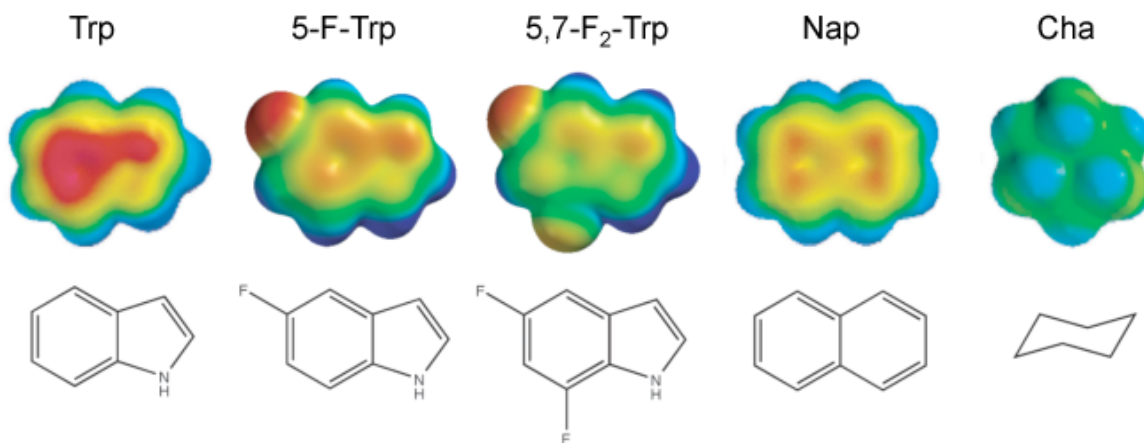
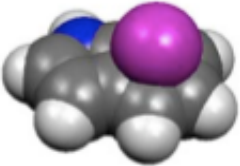


Figure 2.16 Electrostatic potential surfaces for Trp analogs used in the NR2B607 Mg^{2+} binding studies. Stick representations of the side chains are below.

2.2.5 Calculated Magnesium Binding Energies

In previous studies, the calculated *ab initio* binding energy of a Na^+ ion to an aromatic ring was used as a measure of the ring's cation- π binding ability (68, 70) (Figure 2.16). Fluorination of the aromatic ring reduces the cation- π binding ability by reducing the negative electrostatic potential at the center of the ring. In order to verify that nothing unusual occurred with Mg^{2+} , high level *ab initio* calculations were performed using indole and fluorinated derivatives with Mg^{2+} . In the gas phase, the binding of Mg^{2+} to indole gives a ΔE of -142.3 kcal/mol (vs. -32.6 kcal/mol for Na^+). With 5-fluoroindole the affinity is decreased by 11.3 kcal/mol (vs. 5.1 kcal/mol when Na^+ is the probe cation). The cation- π interaction is much stronger for Mg^{2+} than for Na^+ due to the larger charge density on the divalent ion, an anticipated result for an interaction with a large electrostatic component. Fluorination of the side chain also has a greater effect. Similar calculations were performed using implicit solvation models for water, ethanol, and THF (Figure 2.17). The calculations clearly establish that a substantial change would be seen in the results if a direct cation- π interaction were important. For reference, in both the serotonin and γ -aminobutyric acid receptors, the ligands for each receptor (of the type RNH_3^+), resulted in decreased ligand affinity values ranging from 30-fold to 180-fold, respectively (73, 78) to difluorination of a binding site aromatic amino acid.



	Mg²⁺ Binding Energy (kcal/mol)		
	Trp	5-F-Trp	5-F-Trp - Trp
Gas	-142.3	-131.0	11.3
THF	-24.2	-14.8	9.4
EtOH	4.0	11.3	7.3
H₂O	6.7	15.1	8.4

Figure 2.17 Mg^{2+} cation- π binding energies calculated with Trp side chains. Counter-poise corrections were used and all calculations performed at B3LYP/6-31⁺⁺G (d,p) level of theory and basis set.

2.2.6 Mutagenesis studies of Inter-Subunit Contacts in the NMDAR Pore

Previous work demonstrated that only aromatic residues functioned in the pore at NR2B607 (64). However, the results of this study rule out any interaction containing a significant electrostatic component, i.e., the cation- π interaction and π - π interactions. Moreover, a simple hydrophobic side chain such as Leu is not sufficient since the W607L mutation demonstrates no Mg^{2+} block. The W607L mutation also rules out the possibility of the cation- π interaction “jumping” to the NR1 subunit (NR1 W608) when fluorinated derivatives are placed in NR2B. Another explanation is sterics - that a relatively large, flat, hydrophobic side chain is required to “plug” the pore. In order to probe this possibility, several additional Trp analogs were incorporated at NR2B607, 2-Naphthylalanine (2-Nap), Tyr, and cyclohexylalanine (Cha). These Trp analogs are residues used to test steric interactions of the side chain. 2-Nap is structurally similar to Trp but does not contain an indole moiety. Cha is the non-aromatic side chain corresponding to Phe, structurally similar in size and shape to Phe. Incorporation of 2-Nap results in wildtype Mg^{2+} block. Incorporation of Tyr and Cha resulted in an approximate 4-fold shift in Mg^{2+} IC_{50} , but still maintained some receptor block and were essentially identical (Table 2.1). It thus appears that a rigid, relatively flat, hydrophobic residue is required at position 607 for potent Mg^{2+} block.

Table 2.1 IC₅₀ Data for Wild type and Mutant NMDA Receptors. The numbers in parenthesis are the number of oocytes measured to obtain each value. IC₅₀ values, δ values, and K_{0.5} values are shown as mean \pm s.e.m Cation- π binding values are computed as in (64, 70).

Subunit/Amino Acid	Mg ²⁺ IC ₅₀ (μ M) -60 mV	Cation- π Binding (Na ⁺) kcal/mol	n	I Max Avg. (nA)	δ	K _{0.5} (0 mV) (mM)
Wild-type NR1a/2B	76 (\pm 5.5)	32.6	7	850	0.74 (\pm 0.11)	3.7 (\pm 2.9)
NR1a/2B607TAG W	82 (\pm 22)	32.6	6	102	0.77 (\pm 0.07)	11 (\pm 3.2)
NR1a/2B607TAG 2-Nap	37 (\pm 4)	28.9	5	102	0.54 (\pm 0.15)	0.5 (\pm 0.3)
NR1a/2B607TAG 5-F-Trp	52 (\pm 5)	27.5	8	170	0.36 (\pm 0.11)	1.6 (\pm 1.1)
NR1a/2B607TAG 5,7-F2-Trp	52 (\pm 10)	23.3	5	35	0.73 (\pm 0.03)	2.9 (\pm 0.6)
NR1a/2B607TAG Cha	190 (\pm 11)	8.4	4	160	0.39 (\pm 0.06)	1.1 (\pm 0.3)
NR1a/2B607L	No Block		4	510		
NR1a/2B607TAG Y	170 (\pm 28)	26.9	4	1100		
NR1a/NR2BW607R	No Block		4	100		
NR1aR630W/2B	NF					
NR1aR630W/2BW607R	NF					
NR1a/2B607TAG 76mer	No Block		5	25		

2.2.7 Current-Voltage (I-V) Relationships

Since the Mg²⁺ block is voltage-dependent, the agonist-induced current-voltage (I-V) relationships were examined in the presence and absence of Mg²⁺. One way to analyze I-V relationships is by comparing a set of parameters discussed by Woodhull (63). The Woodhull parameters were obtained by plotting the logarithm of the IC₅₀ (LogIC₅₀) over a range of voltage potentials versus the holding potentials. Then a straight line was fit to the data to determine δ and K_{0.5} (Table 2.1). The parameter δ represents the portion of the electric field sensed by the site and K_{0.5} is the half-maximal block at 0 mV. This study determined that wild type NR1a/NR2B receptors demonstrate the expected concentration and voltage dependent Mg²⁺ block (Table 2.1) (79). A mutation that has similar size and cation- π binding ability to Trp, W607 2-Nap, was strongly concentration and voltage dependent. Interestingly, the W607Y mutant does not reach full Mg²⁺ block even though the cation- π binding ability of Tyr is very similar to Trp and 2-Nap (Figure 2.16). This suggests that the voltage-dependent Mg²⁺ block is not correlated to the cation- π binding ability at NR2BW607.

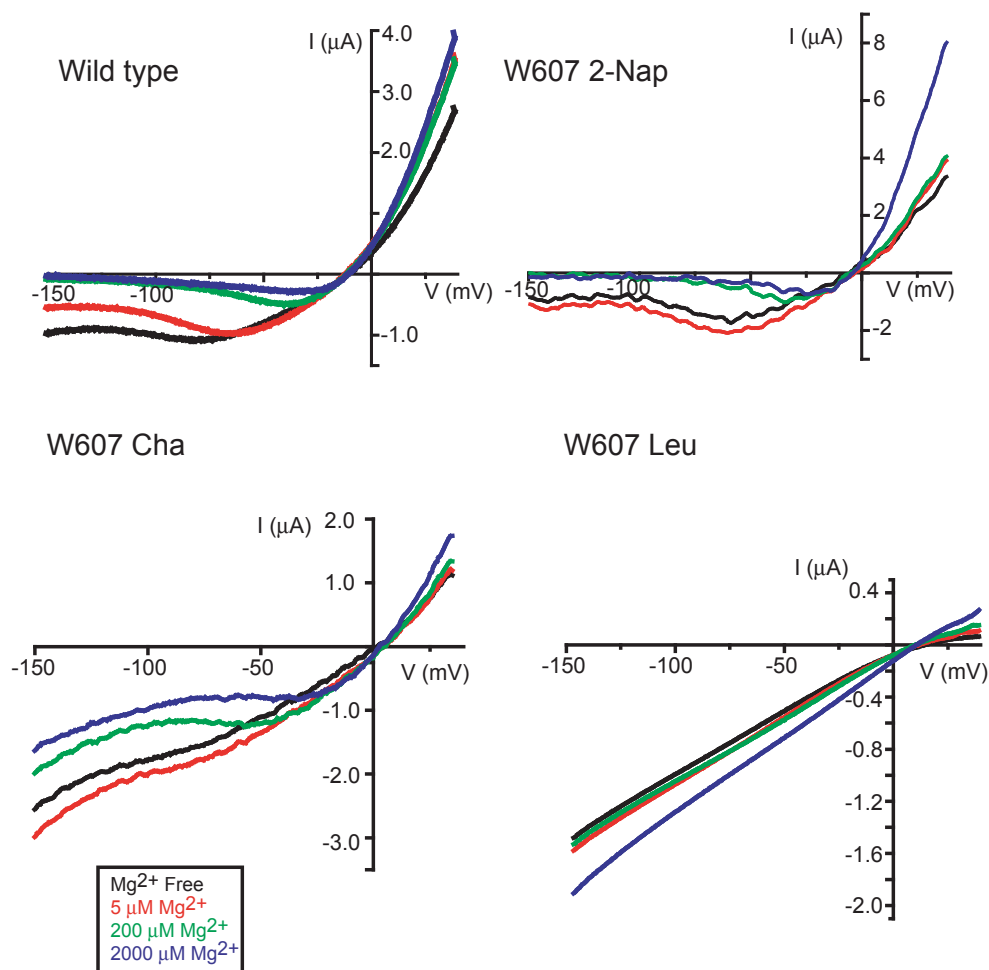


Figure 2.18 Current-voltage (I-V) relations generated by voltage ramps; see methods. NR1a/NR2B, NR1a/NR2BW607 2-Nap, NR1a/NR2BW607 Cha, and NR1a/NR2BW607L.

The voltage-dependence of Mg^{2+} block for the NR2BW607 Cha mutant (Figure 2.18) also was determined. Although the I-V relationship demonstrates some concentration and voltage-dependent Mg^{2+} block of the receptor, the block is incomplete at even the highest Mg^{2+} concentration (2 mM). Additionally, the block is relieved at high negative potentials. This suggests that Mg^{2+} can permeate the pore and block the pore with this mutation. On the other hand, the W607L mutation, also shown in previous studies, displays no relevant Mg^{2+} block at any concentration or voltage tested. From a chemical perspective both Cha and Leu are hydrophobic residues with no significant cation- π ability, yet there are noticeable differences between the Mg^{2+} block of Cha and

Leu. The Cha-containing receptor partially blocks Mg^{2+} , whereas the Leu-containing receptor does not. The experiments conducted in this study suggest that the size and shape of the side chain at NR2B607 influences Mg^{2+} block more than aromaticity.

2.2.8 Similarities of the P-Loop of Glutamate Receptors and Potassium Channels

Since we determined that a cation- π interaction between NR2BW607 and Mg^{2+} doesn't exist, we were interested in investigating other roles for this conserved Trp in channel function. Previous studies and sequence alignments suggest the structural similarity between the pores of potassium channels and glutamate receptors (49) and are often used for modeling purposes when creating images of glutamate receptor overall topology. Sequence comparisons demonstrate a high homology between the pore-forming regions of K^+ channels and the P-loop of glutamate receptors (49, 80), including conservation of the residue that corresponds to NR2BW607. The KcsA K^+ channel corresponding residue, W67 (NR2BW607 equivalent), was identified as being involved in an inter-subunit cation- π interaction with KcsA R49 (Figure 2.19).

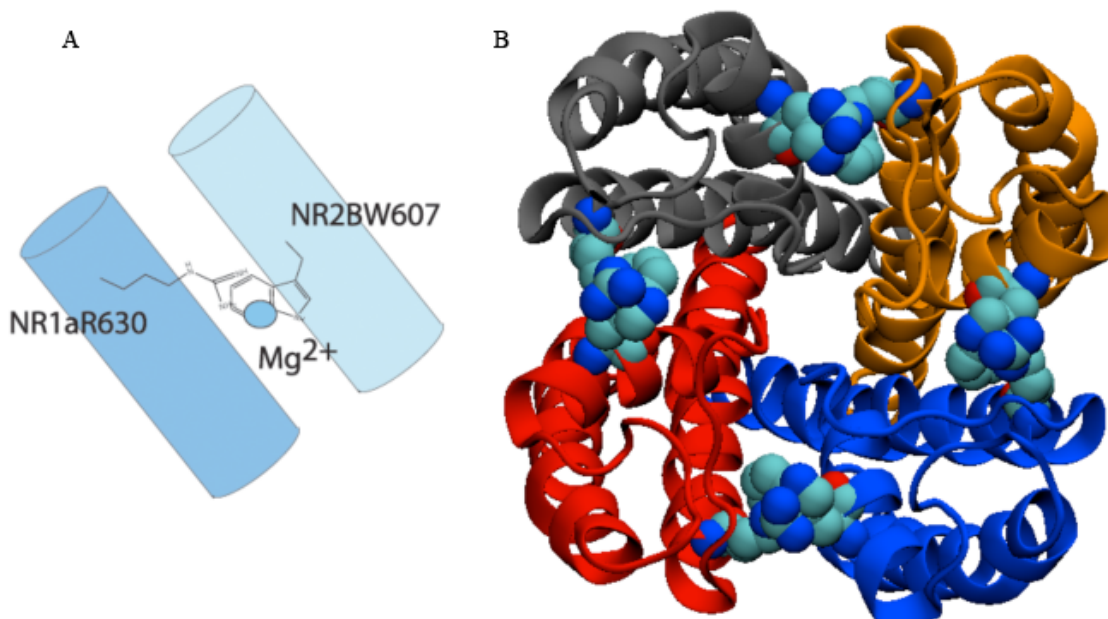


Figure 2.19 Schematic of NMDA receptor pore. A) Schematic demonstrating a possible inter-subunit cation- π interaction between NR1R630 and NR2BW607. B) Crystal structure of KcsA showing the four inter-subunit cation- π interactions between W67 and R49, structure adapted from (81). PDB file: 1BL8.

During the comparison of the receptors, it was noticed that the glutamate receptor residue corresponding to KcsA R49 is either an Arg or Lys, which would be amenable to a cation- π interaction. In order to determine if this inter-subunit interaction translated to the glutamate receptors and to further probe the interaction, “residue swapping” experiments were performed to evaluate NR2BW607R and NR1aR630W mutations and the double mutation. The NR2BW607R mutant activated upon agonist application, but, as expected, the block by extracellular Mg²⁺ was abolished. The NR1aR630W single mutant and NR1aR630W/NR2BW607R double mutant did not produce any current in response to agonist application.

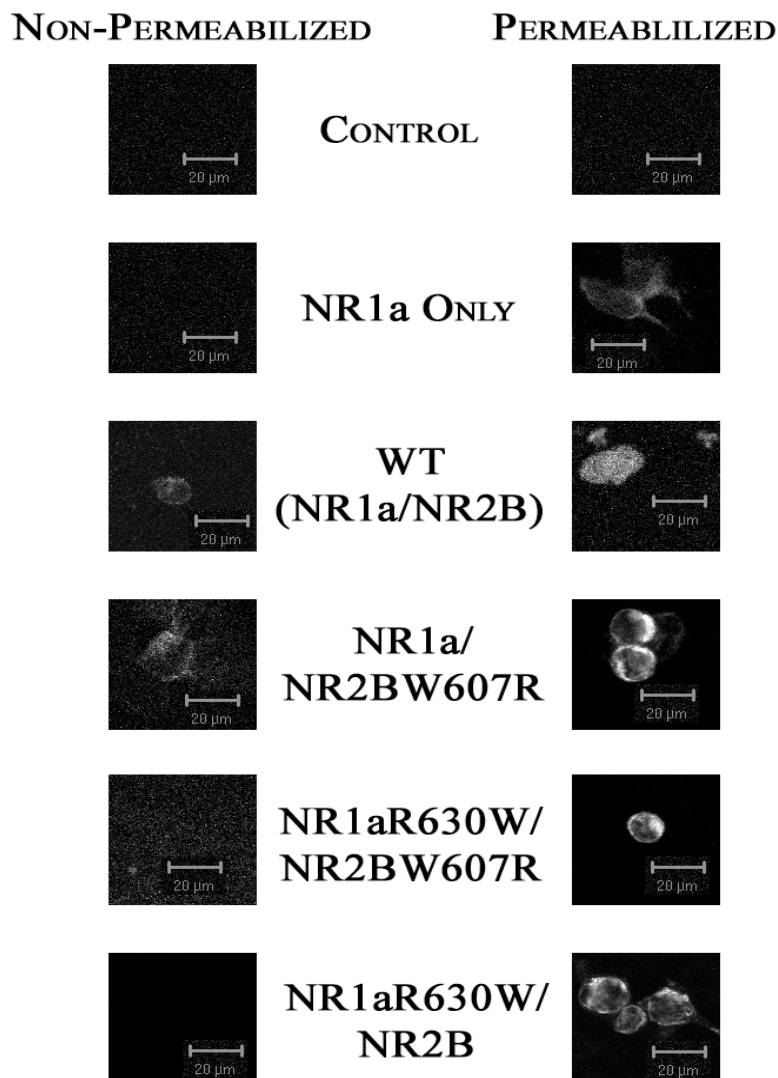


Figure 2.20 Immunolocalization of wild type, functional, and nonfunctional mutant NMDA receptors expressed in HEK293T cells. Permeabilized and non-permeabilized membrane images are labeled.

To determine whether the apparently non-functional mutant receptors were expressing at the plasma membrane, the localization of these mutants was studied using an NR1-specific antibody. HEK293T cells expressing the wild type or the functional mutant (NR1a/NR2BW607R) showed clear labeling of the membrane in non-permeabilized cells. In contrast, no such labeling was seen for the nonfunctional receptor mutants (NR1aR630W/NR2B and NR1aR630W/NR2BW607R) (Figure 2.20). Permeabilization of the membranes allowed labeling of intracellular NR1a subunits in all

cases. While it is possible that expression patterns would be different in HEK293T cells than in *Xenopus* oocytes, we feel the more reasonable explanation is that the receptors that were “nonfunctional” in fact failed to fold and/or transport properly to the cell surface. Although we hypothesized that the double mutant (NR1aR630W/NR2BW607R) might rescue the receptor by re-establishing a cation- π interaction, the results suggest that the Arg at position 630 in NR1a is necessary for receptor assembly and/or transport.

2.2.9 Asparagine Residues and NMDA Receptor Block by Extracellular Cations

After our characterization of the conserved Trp site involved in Mg^{2+} block, this study turned to an investigation of the conserved asparagines in both NMDAR subunits. There are two conserved asparagines in NR2B at positions Asn 615 and Asn 616. Only one exists in the NR1a subunit, Asn 616. By convention, the NR2 subunit N615 is labeled the N site or N(0) site and, N616 is the N+1 site. Previous studies have implicated the asparagine residues in Mg^{2+} block. In addition, these Asn residues are also associated with NMDA receptor block caused by extracellular cations, such as the synthetic small molecules, phencyclidine (PCP), a common drug of abuse, MK-801, an NMDAR antagonist, and memantine (Namenda©), which is a pharmaceutical currently on the market for treatment of moderate to severe Alzheimer’s Disease (82). Using conventional mutagenesis, several studies demonstrated that the Asn residues did not contribute equally to block by external Mg^{2+} (65, 67). As demonstrated in Figure 9, the asparagines are thought to lie at the narrowest constriction of the channel pore and at the top of the P-loop (60), suggesting that one of the side chains can interact more favorably with an extracellular cation compared to the other. Mutagenesis studies in the NR1 and NR2A subunit have demonstrated that the N+1 site contributes to Mg^{2+} block more than the N site (65, 67) of NR2A, while the NR1 subunit Asn contributes very little to Mg^{2+} block.

Keeping in mind the previous studies, this exploration of the N and N+1 sites first focused on the NR2B subunit. Mutagenesis of the Asn residues to Gln, Asp, Ser, and Gly produced evidence that the N+1 site in NR2 provided an energy barrier to ion flux through the channel, establishing a block. Wollmuth *et. al* postulated that the asparagines

could act as a steric block since the size of hydrated Mg^{2+} (> 0.7 nm) would be larger than the pore (0.55 nm). On the other hand, the asparagines could act as a binding site for Mg^{2+} through ion-dipole coordination due to the polarity of the Asn side chain (65). However, one would expect that if the latter were important for Mg^{2+} block, then mutation of the side chain to Asp (full negative charge) would enhance Mg^{2+} block, which was never observed (83, 84). The novel chemical approach used in this study to probe chemical-scale interactions involved incorporation of a series of fluorinated Asns to decrease the side chain polarity. This essentially mirrored the fluorinated Trp experiment, but with a different amino acid side chain.

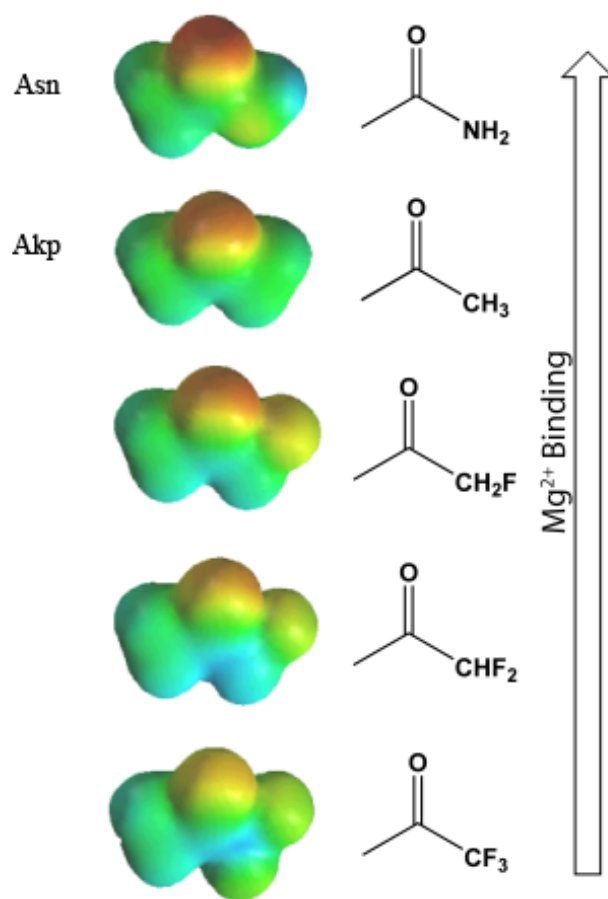


Figure 2.21 Analogs of asparagine that decrease the negative charge density on the amide carbonyl. Electrostatic potential surfaces demonstrate the weaker (less red) amide carbonyl as fluorination of the ketone increases.

The chemistry of Asn would allow the amide carbonyl to chelate Mg^{2+} during NMDAR blockade. The negative electron density would coordinate to Mg^{2+} through an ion-dipole interaction forming an energy barrier to Mg^{2+} release from the pore. This is an ideal interaction to probe chemically. Analogs of Asn that would reduce the negative charge density of the amide carbonyl were sought for incorporation. These analogs would weaken the Mg^{2+} -carbonyl interaction, and it was hoped this would result in a shift in Mg^{2+} IC_{50} . In previous studies of the muscle type nAChR, the neutral Asn analog, 2-amino-4-ketopentanoic acid (Akp, Figure 2.21), was used to delineate the effects of a carbonyl side chain in stabilizing different agonists in the binding site (85-87).

To study the NR2B N and N+1 site residues the N615D, N615TAG, N616Q, N616D, and N616TAG mutations were created. Conventional mutagenesis studies were conducted and resulted in shifts in IC_{50} (Table 2.2). The experiments conducted demonstrated that both the N and N+1 site influenced Mg^{2+} block. Amino acid substitutions at NR2B N615 resulted in no Mg^{2+} block whereas mutations at NR2B N616 resulted in greatly attenuated block. One noticeable shift was the N616D mutation, which slightly decreased IC_{50} . This shift supports previous suggestions that an ion-dipole interaction stabilizes Mg^{2+} block (Table 2.2, Figure 2.22). Following the analysis with conventional mutations, Akp was incorporated at the N and N+1 sites (Table 2.2). The N615Akp mutation resulted in ablation of Mg^{2+} block, whereas the N616Akp mutation produced wild type like Mg^{2+} block. Although these results reinforce the unsymmetrical contribution of the N and N+1 site Asns to Mg^{2+} block, the results of this study suggest that the amide carbonyl of the N site contributes more to Mg^{2+} binding than the N+1 site.

Table 2.2 IC₅₀ values for Mg²⁺ block at the N and N+1 site in NR1a/NR2B NMDA receptors.*The number of oocytes contributing to each IC₅₀ value is in parenthesis.

Mutation	Mg²⁺ (μM)*	Hill
wild type	76.3 ± 5.46 (7)	1.22 ± 0.086
2BN615D	No Block (6)	
2BN615Akp	No Block	
2BN616D	46.3 ± 5.43 (8)	1.06 ± 0.122
2BN616Q	>2000 (5)	
2BN616Akp	~90.0 ± 5 (6)	
1aN616D	607 ± 168 (2)	1.07 ± 0.22
1aN616Q	>3000 (4)	

Following the analysis of Mg²⁺ block for the Asn mutations, an investigation was conducted of the chemical mechanisms of NMDA receptor block by other extracellular cations. Due to the importance of NMDARs in learning and memory and the implications for these receptors in stroke and neurodegenerative diseases, much time and effort already has been spent in an attempt to specifically target and regulate these receptors with small molecules. Memantine (Namenda©) is a cationic NMDAR blocker that reversibly blocks the channel (88, 89). Memantine is often referred to as a “better magnesium ion,” in that it has a higher affinity for the receptor, a slower unblocking rate, and moderate voltage dependence (90-92). Several mutagenesis studies demonstrate that there are two sites of memantine interaction with the NMDARs. The primary binding site occurs at N site Asns, the narrowest constriction of the pore. The secondary binding site is more controversial, but appears to be located in a shallow extracellular vestibule and/or a more extracellular region of the pore (92-97).

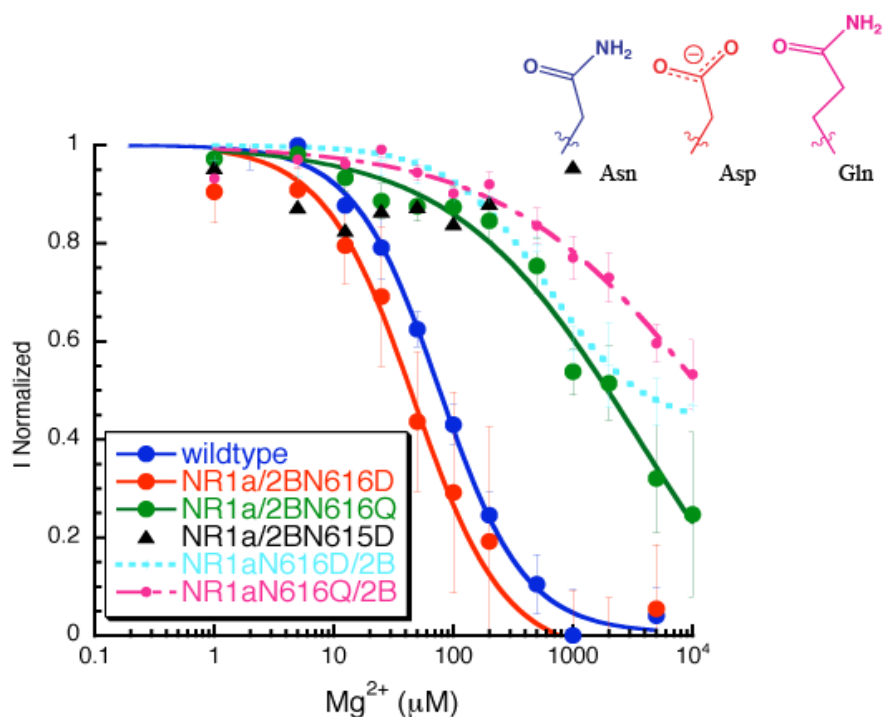


Figure 2.22 Asparagine site IC_{50} curves. IC_{50} dose-response data for NR1a/NR2B receptors with mutations at the N and N+1 sites. Stick representations of the different conventional side chain mutations for the Asp and Gln mutations compared to wild type Asn.

Similar to the Mg^{2+} block, an electrostatic interaction was suspected in the block by memantine. Therefore, parallel experiments were conducted with Asn site mutations to record memantine IC_{50} data. Based on these experiments, memantine is a more potent NMDAR channel blocker with a wild type IC_{50} of 2.4 μM (Figure 2.23). As in previous studies, the NR1a N616Q mutation results in the largest shift in IC_{50} (~10-fold shift) and the NR2 Asn site mutations produce no shift.

After obtaining several IC_{50} values for different N site mutations with both Mg^{2+} and memantine, it was observed that not all of the mutations resulted in full receptor block. This was a concern because the method used for comparing IC_{50} values for the mutations was suspected to not provide an accurate account of the effects these mutations were having on the receptor. For example, several of the mutations do not shift IC_{50} (NR2B N616Q mutation) significantly, but they do greatly attenuate block. Therefore, this study then compared the total amount of receptor block at both the wild type receptor

IC₅₀ value for each blocker and at maximal blocker concentration. Using this method it was expected that large differences in how the mutation affects receptor blockade would be detected.

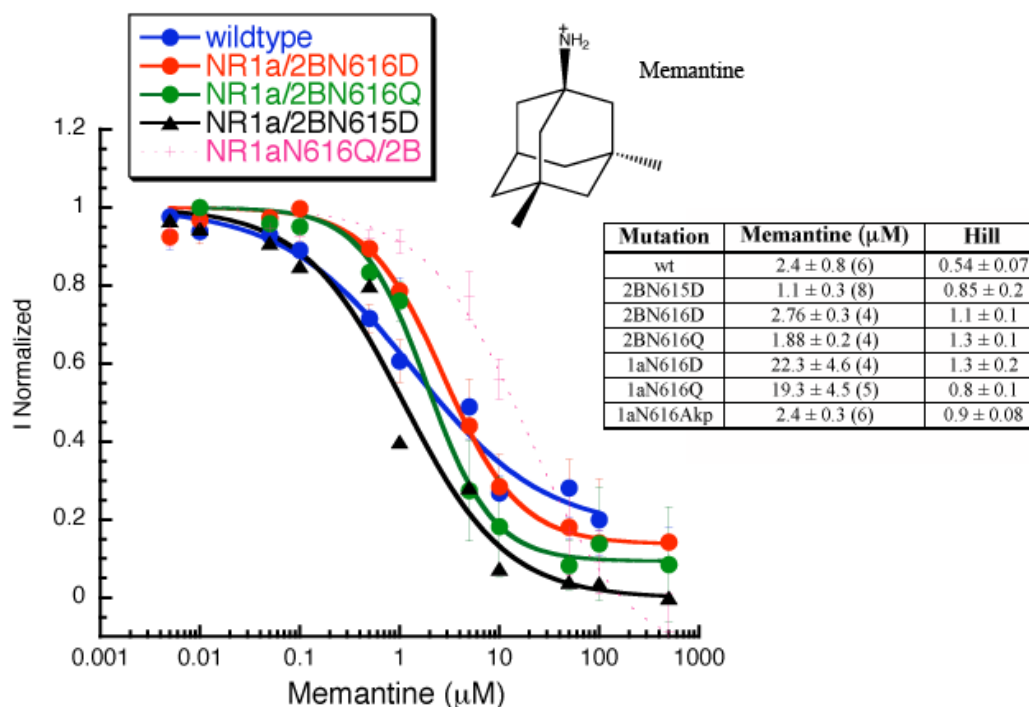


Figure 2.23 Asparagine IC₅₀ curves with memantine. IC₅₀ data for memantine block of wild type (wt) and Asn site mutations in NR1a/NR2B receptors.

This analysis was performed for both Mg²⁺ and memantine block. The overall results suggest that, for Mg²⁺ block, the amide carbonyl of NR2BN615 contributes to Mg²⁺ binding and block. However, altering the sterics of the NR2B N616 side chain with the N616Q mutation resulted in ablation of Mg²⁺ block (Figure 2.24). These results suggest that the size and sterics of the N+1 site contribute to Mg²⁺ block, and that the amide carbonyl of the N site coordinates to the magnesium ion during block. The results with memantine demonstrate that, on the whole, neither the NR2B N or N+1 site contributes to block. In fact, although the block at IC₅₀ levels of memantine varies slightly with the mutations, a large shift is never observed and full receptor block is maintained. These results, combined with those of prior studies using NR1a mutations,

suggest that the N site in the NR1 subunit is involved with memantine block and the NR2B mutations contribute very little to block. Interestingly, these results suggest that these blockers utilize different electrostatic and steric interactions on binding to NMDARs.

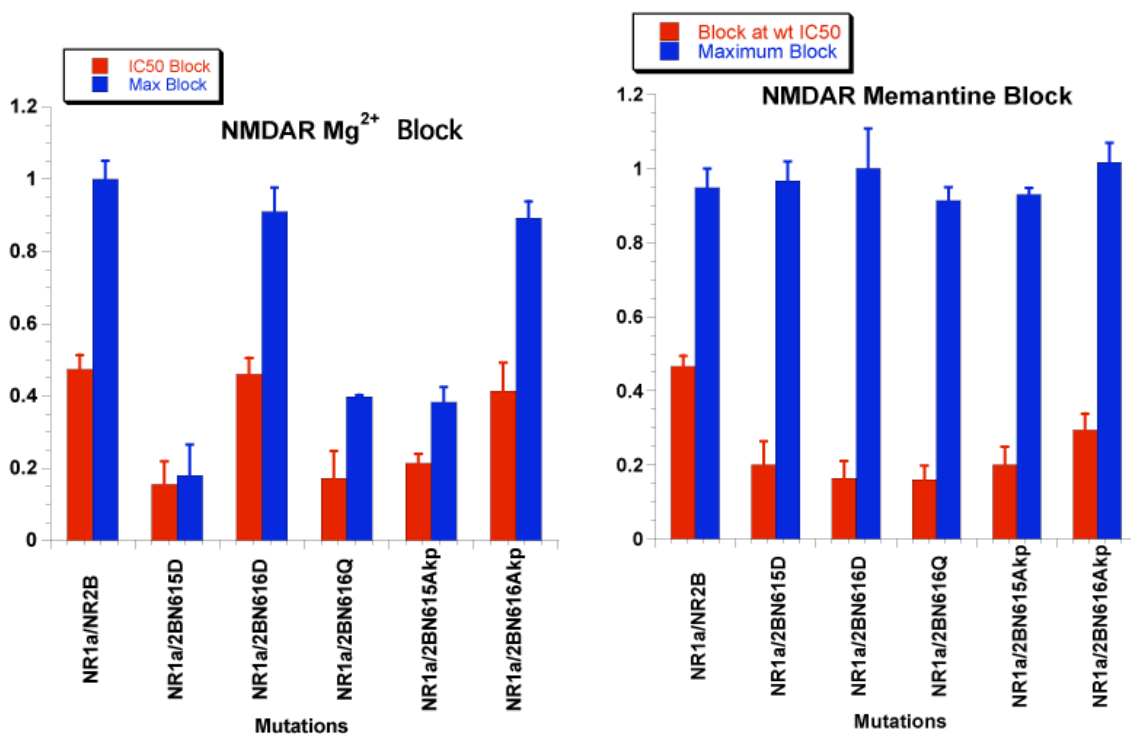


Figure 2.24 Percent block for Mg²⁺ and memantine. Studies of NR1a/NR2B receptor block at N and N+1 site mutations. Receptor block was characterized at wild type IC₅₀ values (red) and at maximal concentrations for Mg²⁺ and memantine (blue).

2.2.10 Additional Studies of NMDA Receptor Blockade

There are many additional molecules that block the NMDA receptors. Investigations of a couple of these were started. MK-801, which is a very potent open channel blocker that binds in the pore of NMDARs, and phencyclidine (PCP), which also binds to and blocks the NMDAR pore, were examined. Both of these molecules are cationic blockers and bind within the pore of NMDARs (Figure 2.25).

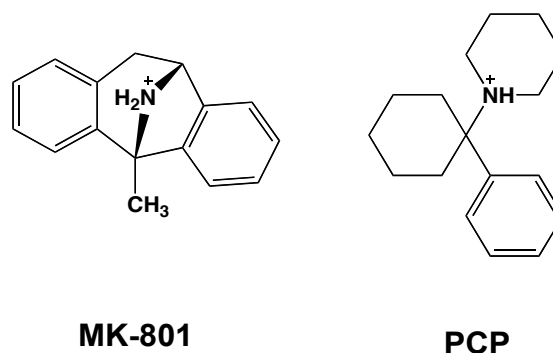


Figure 2.25 NMDA receptor blockers. Structures of the NMDAR blockers MK-801 and PCP.

It quickly became clear that electrophysiology experiments using the OpusXpress would be difficult with MK-801, which is a very potent blocker of the NMDAR and binds at nanomolar concentrations. One issue with MK-801, which also makes it a less than ideal pharmaceutical, is its inability to be “washed off” of the channel. In other words, once it binds to the pore it sticks with such high affinity that it is not removed easily. This can be observed by looking at electrophysiological recordings (Figure 22.26). This feature makes data acquisition very difficult, because in order to generate a dose-response curve, the channel must be reactivated before each dose of blocker is applied. Active channels cannot be reactivated with MK-801 because it remains in the channel. The resulting responses to drug and blocker are not accurate and skew the dose-response relationship, impeding experimentation. Although efforts were made to explore MK-801 further, ultimately these experiments were put aside in place of other experiments.

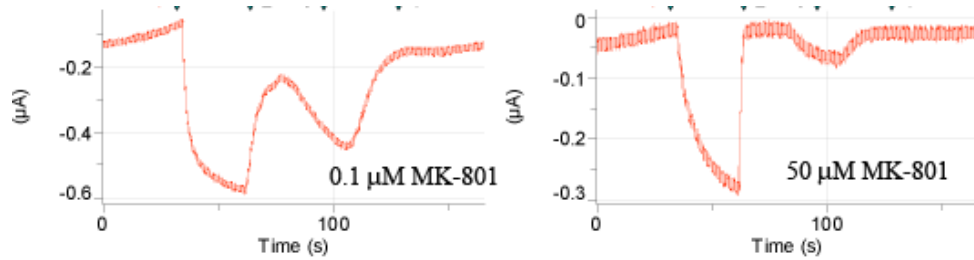


Figure 2.26 Electrophysiology traces from two doses of MK-801. As the concentration of MK-801 increases, more channels remained blocked and channels do not reactivate.

Following the examination of MK-801, the study turned to the blocker PCP. The studies of NR1a/NR2B wild type receptor demonstrated that PCP also is a very potent blocker. The IC_{50} value obtained for wild type receptor block was 204 nM. Two subsequent mutations, NR1a N616Q/NR2B and NR1a/NR2B N615A_{kp}, both shifted PCP IC_{50} by ~ 4 and 7-fold, respectively (Figure 2.27). Although these studies did not conclusively characterize the N and N+1 site Asns in PCP block, the initial results suggest that PCP binds differently than either Mg^{2+} or memantine. Since the N site of both the NR1a and NR2B subunits influences PCP block, it appears that PCP contacts more of the pore. The studies conducted were unable to determine if the PCP block is mostly steric or electrostatic in character. Future studies may be able to clarify this interaction.

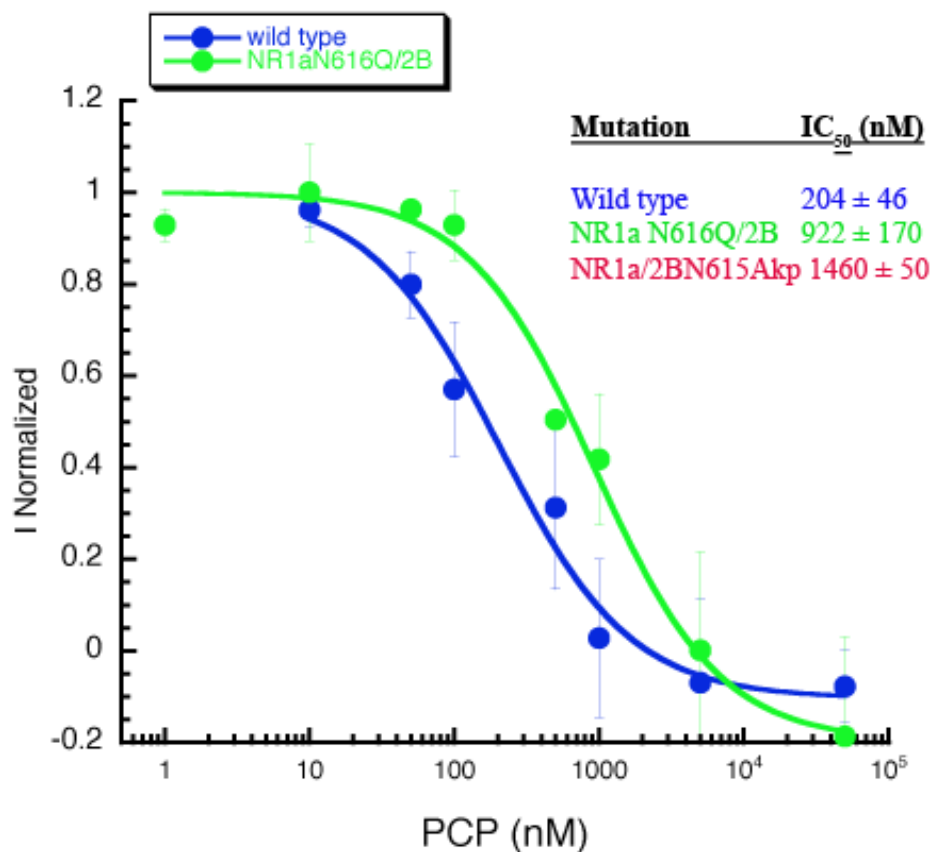


Figure 2.27 PCP IC₅₀ curves. IC₅₀ values for the wild type NR1a/NR2B receptor and two mutations, NR1a N616Q and NR2B N615Akp.

2.3 Discussion and Conclusions

The studies conducted support the conclusion that Mg²⁺ does not interact with the NR2B Trp607 through a cation- π interaction. All previous studies using conventional mutagenesis led to the conclusion that the aromaticity of Trp 607 was crucial for Mg²⁺ blockade. However, the results obtained from employing unnatural amino acid mutagenesis via nonsense suppression have definitively demonstrated that the interaction is not electrostatic in nature. The subtle results of this approach reveal that the more likely interaction that Trp607 is involved in is steric. Simply put, a large, flat residue is required at NR2B 607 (98).

Our studies with several different side chains support the idea that structural requirements at W607 are necessary to maintain Mg²⁺ block. For example, large, flat

side chains such as Trp, 2-Nap, F₂-Trp, and Cha all maintain levels of Mg²⁺ block similar to the wild type receptors. At the same time, we also noticed subtler effects on Mg²⁺ block such as the incorporation of Tyr and Cha, which seem to distort the receptor pore enough for incomplete Mg²⁺ block (although it can be relieved at high negative potentials). This implies that the size and/or shape of the Tyr or Cha side chains at position 607 does subtly distort the pore, so that Mg²⁺ can permeate more easily. Additionally, the W607Cha data would suggest that an aromatic residue is not absolutely necessary for receptor function, since partial block is observed in these channels. It is reasonable to suggest that the important features of the Trp residue are its size, shape, and hydrophobicity, which allow it to fit into the channel architecture to create the desired Mg²⁺ block during NMDA receptor function (98).

In studies conducted of the Mg²⁺ block we have demonstrated that the conserved N and N+1 site Asn residues in both NR1a and NR2B are important during Mg²⁺ block. Prior studies suggested that the two NR2 sites do not contribute equally to Mg²⁺ block. Conventional mutagenesis studies concluded that the NR2 N+1 site contributed to Mg²⁺ block more than the N site of either subunit. By using the unnatural amino acid mutagenesis technique, the importance of the amide carbonyl of Asn could be tested in an electrostatic interaction with the metal cation. The experiments conducted, incorporating the unnatural amino acid Akp, suggest that the amide carbonyl of NR2B N615 (N site) is more important for Mg²⁺ block than the amide carbonyl of the N+1 site. At the same time, the conventional mutagenesis experiments also demonstrated the importance of the N+1 site in Mg²⁺ block. Combining these studies it is suggested that although the N+1 site Asn may provide a steric component to Mg²⁺ block (it is thought to lie at the narrowest constriction of the pore), the N site may coordinate to Mg²⁺ through an ion-dipole interaction.

The studies of the pore Asns also provided interesting suggestions about the mechanism of memantine block of the NR1a/NR2B receptor. Memantine block is complicated since there is a proposed primary and secondary binding site (90, 92). Instead of the NR2 subunit Asns contributing to memantine block via electrostatic interactions, the mutation with the most dramatic influence on memantine block was NR1a N616Q. None of the other mutations at either site in NR2B resulted in a

substantial shift in receptor blockade, likely suggesting that these are not the only chemical interactions at play between the receptor and memantine during block. Previous studies by the Lipton group have postulated that several binding sites for memantine exist in and around the NMDAR pore (92). This can complicate mutagenesis studies because as one set of NMDAR-memantine interactions is altered, other important interactions between the receptor and blocker can (and likely do) compensate for the mutations. However, the more subtle mutations, inherent in the technique used here, provide precise evidence of the molecular nature of the interactions involved in memantine block. These distinguish memantine block from Mg^{2+} block. It is likely that Mg^{2+} interacts with the amide carbonyl via an electrostatic interaction of the NR2B N site while memantine seems not to be influenced by the NR2B subunit at all during receptor block. The use of unnatural amino acid mutagenesis has revealed that Mg^{2+} and memantine, although both cationic blockers, interact with the NMDAR pore via different mechanisms.

The results of this study and prior studies demonstrate the limits of current understanding of the action of cations in blocking the pore of NMDA receptors. Additionally, recent evidence suggests that the pore region may not be the only area of the protein involved in receptor blockade. Contributions from the LBD also may influence the structure of the pore and how different cations interact in the pore domain (99). This area of research is ongoing and provides a prime example for how biophysical chemistry on the molecular scale contributes unique insights and understanding of these complex biological processes. Several lab members, including Walrati Limapichat and Wesley Yu, will continue future studies of the mechanism of block by memantine.

These experiments demonstrate that a new family of neuroreceptors (iGluRs), the NMDA receptor in particular, is amenable to study using unnatural amino acid mutagenesis. Now that a protocol has been established for use of the nonsense suppression methodology to incorporate unnatural amino acids into these highly important receptors, the role of many chemical interactions involved in their structure and function can be explored.

Chapter 3 will examine how this methodology has been used to focus on a different domain of the NMDAR, the ligand-binding domain. Also, the efforts to expand the methodology into another iGluR subfamily, the AMPA receptors, will be described. Because glutamate receptors in general and, specifically, NMDA receptors, play such an integral role in many neuronal functions and diseases due mostly to their high Ca^{2+} permeability, they are an incredibly interesting set of neuroreceptors for exploration. The long-term goal of these efforts is to study these receptors in a mammalian cell system and explore how their structure and function interplay with different neuronal signaling cascades within the cell.

2.4 Materials and Methods

2.4.1 Molecular Biology

The NR1a and NR2B subunits were subcloned from pBluescript into pAMV (100) for increased expression in *Xenopus laevis* oocytes. For the NR1a subcloning, primers complimentary to the 5' and 3' ends of the gene were synthesized (Integrated DNA Technologies), the gene was amplified using PCR, and then subcloned into the pAMV vector using the *NcoI* and *BamHI* restriction enzymes and DNA ligase. The NR2B subcloning was more involved. Initially, the first 1.5 kb of the NR2B subunit (from the 5' end) was amplified using PCR and subcloned into pAMV utilizing overlapping primers and PCR. The overlapping primers were constructed using 12 amino acids from the AMV sequence that directly preceded the start codon of the plasmid and the first 12 amino acids from the NR2B gene (72 bp/primer). The second 3.0 kb of NR2B were subcloned into the modified pAMV containing 1.5 kb from NR2B by restriction digestion between the plasmid and the fragment (3.0 kb) using *BamHI* and *AflIII* and ligating with T4 DNA Ligase (Figure 2.28).

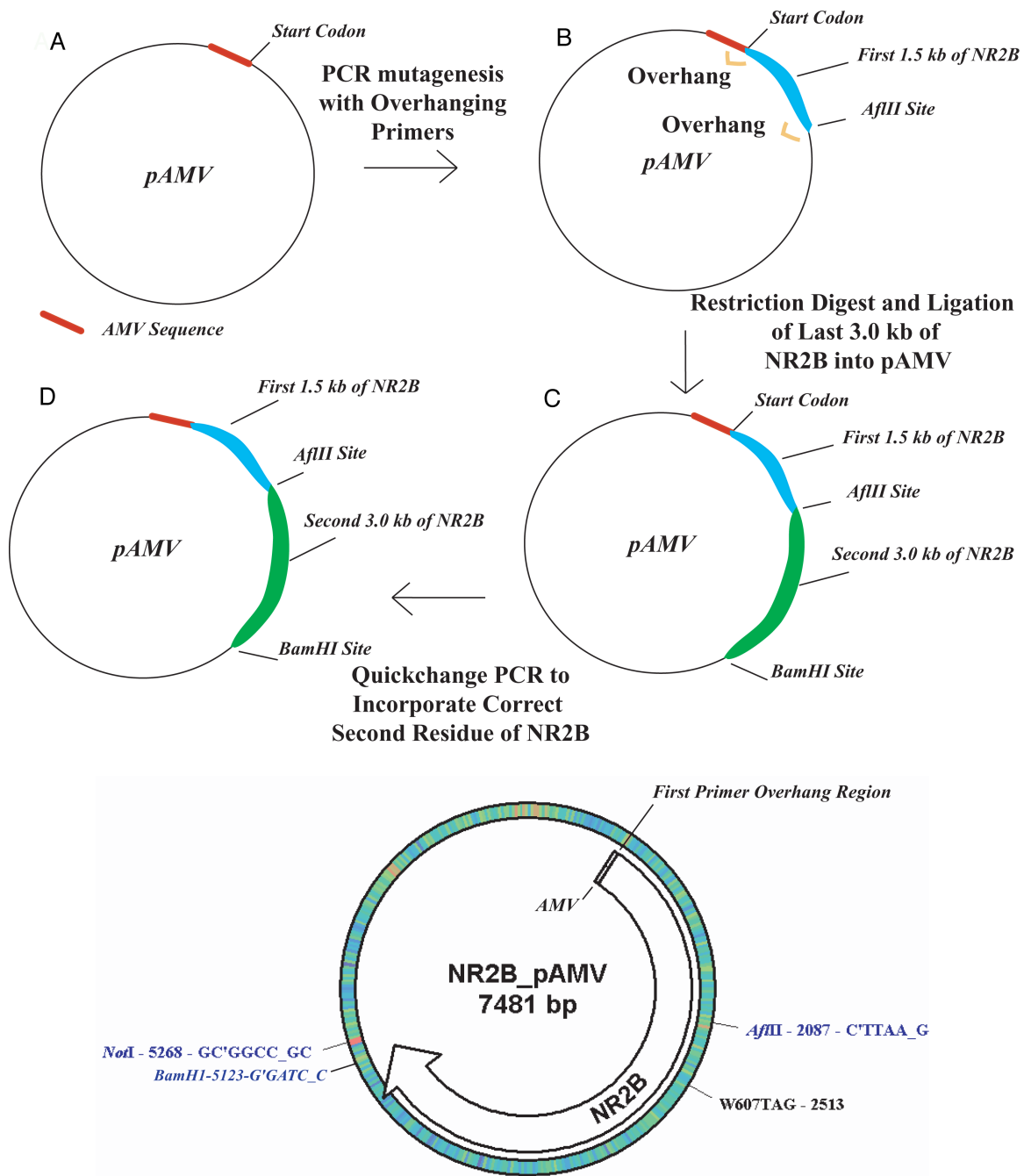


Figure 2.28 NMDA receptor cloning. Cloning schematic for NR2B insertion into *pAMV* from *pBluescript*. Final vector map of NR2B in *pAMV* with the TAG (stop) codon inserted at site 607.

Mutant NR1a and NR2B subunits were prepared by site-directed mutagenesis. All mutant and wild type cDNA was linearized with *NotI* and mRNA was synthesized by

in vitro runoff transcription using the T7 mMESSAGE mMACHINE kit (Ambion). Conventional mutants and wild type mRNA were injected in a NR1a:NR2B (1:5) ratio. Synthetic amino acids were ligated to truncated 74 nt tRNA as described previously (100). The aminoacyl tRNA was deprotected by photolysis immediately prior to co-injection with mRNA. Typically, 5 ng mRNA and 25 ng tRNA-aa were injected into oocytes in a total volume of 50 nL. To increase expression of suppressed receptors, 1 day after the first injection a “booster” of 25 ng tRNA-aa was given and the cells incubated one additional day before electrophysiological measurements were made (48 hours total).

2.4.2 Electrophysiology

Stage V-VI *Xenopus laevis* oocytes were injected with 50nL/cell of mRNA/tRNA mixtures. Oocytes were evaluated in a Mg^{2+} and Ca^{2+} free saline solution (96 mM NaCl, 5 mM HEPES, 2 mM KCl, 1 mM $BaCl_2$). The receptors were activated in a Mg^{2+} and Ca^{2+} free solution containing 100mM glutamate (Aldrich), 10 mM glycine (Aldrich), and 100 mM niflumic acid (to reduce activity of Ca^{2+} activated Cl^- channels, Sigma). All oocyte recordings were made 48 hours after initial injection in two-electrode voltage clamp mode using the OpusXpress 6000A (Molecular Devices). Solutions were superfused at flow rates of 1 and 4 mL/min during Mg^{2+} application and 3 mL/min during wash. Eight oocytes were simultaneously voltage clamped at -60 mV and dose-response relationships were obtained by delivery of various concentrations of Mg^{2+} in 1 mL aliquots. The data were analyzed using the Clampfit 9.0 software (Axon).

The Hill equation was used to fit data: $I/I_{max}=1/(1+(IC_{50}/[A])^{n_H})$, where I is peak current at drug concentration (A), IC_{50} is the concentration of drug that inhibits 50% of the maximal response, and n_H is the Hill coefficient. Voltage ramps (-150 mV to $+40$ mV during 4 s) were used to construct I–V curves for (glutamate and glycine)-evoked conductance in the presence and absence of Mg^{2+} . Leak currents measured in the absence of glutamate, glycine, niflumic acid, and Mg^{2+} were subtracted. The voltage dependence of block (δ , fraction of the electric field that the blocker experiences) and the affinity of Mg^{2+} at 0 mV ($K_{0.5}$) were calculated by determining the IC_{50} at varying potentials (-40 to -100 mV). The logarithm of IC_{50} was plotted against the holding potentials and a straight line was fitted to the data to determine δ and $K_{0.5}$. The δ and $K_{0.5}$ were calculated

according to Woodhull (63): $K_{0.5}(V) = K_{0.5} \times \exp(zdVF/RT)$, V is membrane potential, z is valence, R , T , and F have their traditional meaning. For the Mg^{2+} and memantine block experiments, we measured % block at wild type IC_{50} levels by measuring the amount of whole-cell current generated for each mutation (induced by glutamate and glycine application) and the amount of current that was blocked by a dose of Mg^{2+} or memantine at the IC_{50} value (determined for wild type receptor) of each blocker. We determined the amount of current that was blocked vs. the amount of current generated by agonist application. This was done for many oocytes and the amount of block was averaged. Before plotting, we determined % block by subtracting the amount of block from 1. To determine the % maximal block we used the largest concentration of either Mg^{2+} or memantine and used the same analysis previously described.

2.4.3 Immunolocalization of Wild type and Mutant NMDA Receptors.

These experiments were performed by adapting previously reported procedures (101, 102). HEK293T cells were calcium phosphate transfected with 10 ng of cDNA. Cells were incubated at 37°C for 2 days. Transfected cells were washed with Tris-buffered saline (3x) and fixed using ice-cold 4% paraformaldehyde in phosphate buffer. The receptors were labeled with anti-NMDAR1 clone 54.1 (Zymed) at a 1:100 dilution in phosphate-buffered saline. Inclusion of 0.3% Triton X-100 permeabilized the membranes for detection of intracellular receptor expression. The cells were incubated with primary antibody for 1 hour at room temperature. Cells were washed (3x) with phosphate-buffered saline. Biotinylated anti-mouse IgG (Vector) was added to the cells and incubated for 1 hour and then rinsed (3x) with phosphate-buffered saline. Fluorescein isothiocyanate avidin D (Vector) was then added to the cells and incubated for 1 hour. Coverslips were mounted in Vectashield mounting medium (Vector) and immunofluorescence was observed using a confocal microscope.

2.4.4. Computational Modeling

The indole-Mg²⁺ complex in Figure 16 and the analogous 5-F-indole complex were optimized at B3LYP/6-31⁺⁺G (d,p) level of theory. The geometries were optimized and fully characterized as minima by analysis of frequency. Energies were calculated at the B3LYP/6-31⁺⁺G (d,p) level. Additionally, basis set superposition error (BSSE) corrections were determined in the gas phase at the B3LYP/6-31⁺⁺G (d,p) level using the counterpoise correction method from Boys and Bernardi (103). All calculations were performed with the Gaussian 98 program (104).

2.5 Cited References

1. Neves, G., Cooke, S. F., and Bliss, T. V. (2008) Synaptic plasticity, memory and the hippocampus: a neural network approach to causality, *Nat Rev Neurosci* 9, 65-75.
2. Collingridge, G. L., Isaac, J. T., and Wang, Y. T. (2004) Receptor trafficking and synaptic plasticity, *Nat Rev Neurosci* 5, 952-962.
3. Lomo, T. (2003) The discovery of long-term potentiation, *Philos Trans R Soc Lond B Biol Sci* 358, 617-620.
4. Andersen, P., Andersson, S. A., and Lomo, T. (1966) Patterns of spontaneous rhythmic activity within various thalamic nuclei, *Nature* 211, 888-889.
5. Douglas, R. M., and Goddard, G. V. (1975) Long-term potentiation of the perforant path-granule cell synapse in the rat hippocampus, *Brain Res* 86, 205-215.
6. Lamprecht, R., and LeDoux, J. (2004) Structural plasticity and memory, *Nat Rev Neurosci* 5, 45-54.
7. Yasuda, H., Barth, A. L., Stellwagen, D., and Malenka, R. C. (2003) A developmental switch in the signaling cascades for LTP induction, *Nat Neurosci* 6, 15-16.
8. Malenka, R. C., and Bear, M. F. (2004) LTP and LTD: an embarrassment of riches, *Neuron* 44, 5-21.
9. Malenka, R. C. (2003) The long-term potential of LTP, *Nat Rev Neurosci* 4, 923-926.
10. Frey, U., and Morris, R. G. (1997) Synaptic tagging and long-term potentiation, *Nature* 385, 533-536.
11. Shi, S. H., Hayashi, Y., Petralia, R. S., Zaman, S. H., Wenthold, R. J., Svoboda, K., and Malinow, R. (1999) Rapid spine delivery and redistribution of AMPA receptors after synaptic NMDA receptor activation, *Science* 284, 1811-1816.
12. Malinow, R., and Malenka, R. C. (2002) AMPA receptor trafficking and synaptic plasticity, *Annu Rev Neurosci* 25, 103-126.
13. Liu, S. Q., and Cull-Candy, S. G. (2000) Synaptic activity at calcium-permeable AMPA receptors induces a switch in receptor subtype, *Nature* 405, 454-458.
14. Brecht, D. S., and Nicoll, R. A. (2003) AMPA receptor trafficking at excitatory synapses, *Neuron* 40, 361-379.
15. Dingledine, R., Borges, K., Bowie, D., and Traynelis, S. F. (1999) The glutamate receptor ion channels, *Pharmacol Rev* 51, 7-61.
16. Schmitz, D., Mellor, J., Breustedt, J., and Nicoll, R. A. (2003) Presynaptic kainate receptors impart an associative property to hippocampal mossy fiber long-term potentiation, *Nat Neurosci* 6, 1058-1063.
17. Bortolotto, Z. A., Lauri, S., Isaac, J. T., and Collingridge, G. L. (2003) Kainate receptors and the induction of mossy fibre long-term potentiation, *Philos Trans R Soc Lond B Biol Sci* 358, 657-666.
18. Song, I., and Haganir, R. L. (2002) Regulation of AMPA receptors during synaptic plasticity, *Trends Neurosci* 25, 578-588.
19. Malenka, R. C. (2003) Synaptic plasticity and AMPA receptor trafficking, *Ann N Y Acad Sci* 1003, 1-11.

20. Santos, S. D., Carvalho, A. L., Caldeira, M. V., and Duarte, C. B. (2009) Regulation of AMPA receptors and synaptic plasticity, *Neuroscience* 158, 105-125.
21. Lisman, J., and Raghavachari, S. (2006) A unified model of the presynaptic and postsynaptic changes during LTP at CA1 synapses, *Sci STKE* 2006, re11.
22. Malinow, R., Mainen, Z. F., and Hayashi, Y. (2000) LTP mechanisms: from silence to four-lane traffic, *Curr Opin Neurobiol* 10, 352-357.
23. Sweatt, J. D. (1999) Toward a molecular explanation for long-term potentiation, *Learn Mem* 6, 399-416.
24. Benke, T. A., Luthi, A., Isaac, J. T., and Collingridge, G. L. (1998) Modulation of AMPA receptor unitary conductance by synaptic activity, *Nature* 393, 793-797.
25. Kennedy, M. B., Beale, H. C., Carlisle, H. J., and Washburn, L. R. (2005) Integration of biochemical signalling in spines, *Nat Rev Neurosci* 6, 423-434.
26. Barry, M. F., and Ziff, E. B. (2002) Receptor trafficking and the plasticity of excitatory synapses, *Curr Opin Neurobiol* 12, 279-286.
27. Kennedy, M. B. (2000) Signal-processing machines at the postsynaptic density, *Science* 290, 750-754.
28. Greger, I. H., Ziff, E. B., and Penn, A. C. (2007) Molecular determinants of AMPA receptor subunit assembly, *Trends Neurosci* 30, 407-416.
29. Greger, I. H., and Esteban, J. A. (2007) AMPA receptor biogenesis and trafficking, *Curr Opin Neurobiol* 17, 289-297.
30. Mayer, M. L. (2005) Glutamate receptor ion channels, *Curr Opin Neurobiol* 15, 282-288.
31. Eriksson, M., Nilsson, A., Samuelsson, H., Samuelsson, E. B., Mo, L., Akesson, E., Benedikz, E., and Sundstrom, E. (2007) On the role of NR3A in human NMDA receptors, *Physiol Behav* 92, 54-59.
32. Wood, P. L. (1995) The co-agonist concept: is the NMDA-associated glycine receptor saturated in vivo?, *Life Sci* 57, 301-310.
33. Sommer, B., Kohler, M., Sprengel, R., and Seeburg, P. H. (1991) RNA editing in brain controls a determinant of ion flow in glutamate-gated channels, *Cell* 67, 11-19.
34. Egebjerg, J., Kukekov, V., and Heinemann, S. F. (1994) Intron sequence directs RNA editing of the glutamate receptor subunit GluR2 coding sequence, *Proc Natl Acad Sci U S A* 91, 10270-10274.
35. Sommer, B., Keinänen, K., Verdoorn, T. A., Wisden, W., Burnashev, N., Herb, A., Kohler, M., Takagi, T., Sakmann, B., and Seeburg, P. H. (1990) Flip and flop: a cell-specific functional switch in glutamate-operated channels of the CNS, *Science* 249, 1580-1585.
36. Mosbacher, J., Schoepfer, R., Monyer, H., Burnashev, N., Seeburg, P. H., and Ruppertsberg, J. P. (1994) A molecular determinant for submillisecond desensitization in glutamate receptors, *Science* 266, 1059-1062.
37. Sheng, M., Cummings, J., Roldan, L. A., Jan, Y. N., and Jan, L. Y. (1994) Changing subunit composition of heteromeric NMDA receptors during development of rat cortex, *Nature* 368, 144-147.

38. Monyer, H., Burnashev, N., Laurie, D. J., Sakmann, B., and Seeburg, P. H. (1994) Developmental and regional expression in the rat brain and functional properties of four NMDA receptors, *Neuron* 12, 529-540.
39. Buller, A. L., and Monaghan, D. T. (1997) Pharmacological heterogeneity of NMDA receptors: characterization of NR1a/NR2D heteromers expressed in *Xenopus* oocytes, *Eur J Pharmacol* 320, 87-94.
40. Hollmann, M., and Heinemann, S. (1994) Cloned glutamate receptors, *Annu Rev Neurosci* 17, 31-108.
41. Nakagawa, T., Cheng, Y., Ramm, E., Sheng, M., and Walz, T. (2005) Structure and different conformational states of native AMPA receptor complexes, *Nature* 433, 545-549.
42. Kunishima, N., Shimada, Y., Tsuji, Y., Sato, T., Yamamoto, M., Kumasaka, T., Nakanishi, S., Jingami, H., and Morikawa, K. (2000) Structural basis of glutamate recognition by a dimeric metabotropic glutamate receptor, *Nature* 407, 971-977.
43. Jin, R., Singh, S. K., Gu, S., Furukawa, H., Sobolevsky, A. I., Zhou, J., Jin, Y., and Gouaux, E. (2009) Crystal structure and association behaviour of the GluR2 amino-terminal domain, *EMBO J* 28, 1812-1823.
44. Jin, R., Banke, T. G., Mayer, M. L., Traynelis, S. F., and Gouaux, E. (2003) Structural basis for partial agonist action at ionotropic glutamate receptors, *Nat Neurosci* 6, 803-810.
45. Gouaux, E. (2004) Structure and function of AMPA receptors, *J Physiol* 554, 249-253.
46. Furukawa, H., Singh, S. K., Mancusso, R., and Gouaux, E. (2005) Subunit arrangement and function in NMDA receptors, *Nature* 438, 185-192.
47. Furukawa, H., and Gouaux, E. (2003) Mechanisms of activation, inhibition and specificity: crystal structures of the NMDA receptor NR1 ligand-binding core, *EMBO J* 22, 2873-2885.
48. Armstrong, N., Sun, Y., Chen, G. Q., and Gouaux, E. (1998) Structure of a glutamate-receptor ligand-binding core in complex with kainate, *Nature* 395, 913-917.
49. Wood, M. W., VanDongen, H. M., and VanDongen, A. M. (1995) Structural conservation of ion conduction pathways in K channels and glutamate receptors, *Proc Natl Acad Sci U S A* 92, 4882-4886.
50. Rosenmund, C., Stern-Bach, Y., and Stevens, C. F. (1998) The tetrameric structure of a glutamate receptor channel, *Science* 280, 1596-1599.
51. Bennett, J. A., and Dingledine, R. (1995) Topology profile for a glutamate receptor: three transmembrane domains and a channel-lining reentrant membrane loop, *Neuron* 14, 373-384.
52. Kumar, J., Schuck, P., Jin, R., and Mayer, M. L. (2009) The N-terminal domain of GluR6-subtype glutamate receptor ion channels, *Nat Struct Mol Biol*.
53. O'Hara, P. J., Sheppard, P. O., Thogersen, H., Venezia, D., Haldeman, B. A., McGrane, V., Houamed, K. M., Thomsen, C., Gilbert, T. L., and Mulvihill, E. R. (1993) The ligand-binding domain in metabotropic glutamate receptors is related to bacterial periplasmic binding proteins, *Neuron* 11, 41-52.

54. Nowak, L., Bregestovski, P., Ascher, P., Herbet, A., and Prochiantz, A. (1984) Magnesium gates glutamate-activated channels in mouse central neurones, *Nature* 307, 462-465.
55. Mayer, M. L., Westbrook, G. L., and Guthrie, P. B. (1984) Voltage-dependent block by Mg^{2+} of NMDA responses in spinal cord neurones, *Nature* 309, 261-263.
56. Li-Smerin, Y., and Johnson, J. W. (1996) Effects of intracellular Mg^{2+} on channel gating and steady-state responses of the NMDA receptor in cultured rat neurons, *J Physiol* 491 (Pt 1), 137-150.
57. Mori, H., Masaki, H., Yamakura, T., and Mishina, M. (1992) Identification by mutagenesis of a $Mg(2+)$ -block site of the NMDA receptor channel, *Nature* 358, 673-675.
58. Ascher, P., and Nowak, L. (1988) The role of divalent cations in the N-methyl-D-aspartate responses of mouse central neurones in culture, *J Physiol* 399, 247-266.
59. Antonov, S. M., and Johnson, J. W. (1999) Permeant ion regulation of N-methyl-D-aspartate receptor channel block by $Mg(2+)$, *Proc Natl Acad Sci U S A* 96, 14571-14576.
60. Wollmuth, L. P., Kuner, T., Seeburg, P. H., and Sakmann, B. (1996) Differential contribution of the NR1- and NR2A-subunits to the selectivity filter of recombinant NMDA receptor channels, *J Physiol* 491 (Pt 3), 779-797.
61. Villarroel, A., Burnashev, N., and Sakmann, B. (1995) Dimensions of the narrow portion of a recombinant NMDA receptor channel, *Biophys J* 68, 866-875.
62. Zhou, Y., Morais-Cabral, J. H., Kaufman, A., and MacKinnon, R. (2001) Chemistry of ion coordination and hydration revealed by a K^+ channel-Fab complex at 2.0 Å resolution, *Nature* 414, 43-48.
63. Woodhull, A. M. (1973) Ionic blockage of sodium channels in nerve, *J Gen Physiol* 61, 687-708.
64. Williams, K., Pahk, A. J., Kashiwagi, K., Masuko, T., Nguyen, N. D., and Igarashi, K. (1998) The selectivity filter of the N-methyl-D-aspartate receptor: a tryptophan residue controls block and permeation of Mg^{2+} , *Mol Pharmacol* 53, 933-941.
65. Wollmuth, L. P., Kuner, T., and Sakmann, B. (1998) Adjacent asparagines in the NR2-subunit of the NMDA receptor channel control the voltage-dependent block by extracellular Mg^{2+} , *J Physiol* 506 (Pt 1), 13-32.
66. Kupper, J., Ascher, P., and Neyton, J. (1998) Internal Mg^{2+} block of recombinant NMDA channels mutated within the selectivity filter and expressed in *Xenopus* oocytes, *J Physiol* 507 (Pt 1), 1-12.
67. Burnashev, N., Schoepfer, R., Monyer, H., Ruppertsberg, J. P., Gunther, W., Seeburg, P. H., and Sakmann, B. (1992) Control by asparagine residues of calcium permeability and magnesium blockade in the NMDA receptor, *Science* 257, 1415-1419.
68. Zhong, W., Gallivan, J. P., Zhang, Y., Li, L., Lester, H. A., and Dougherty, D. A. (1998) From ab initio quantum mechanics to molecular neurobiology: a cation- π binding site in the nicotinic receptor, *Proc Natl Acad Sci U S A* 95, 12088-12093.

69. Mu, T. W., Lester, H. A., and Dougherty, D. A. (2003) Different binding orientations for the same agonist at homologous receptors: a lock and key or a simple wedge?, *J Am Chem Soc* 125, 6850-6851.
70. Mecozzi, S., West, A. P., Jr., and Dougherty, D. A. (1996) Cation-pi interactions in aromatics of biological and medicinal interest: electrostatic potential surfaces as a useful qualitative guide, *Proc Natl Acad Sci U S A* 93, 10566-10571.
71. Dougherty, D. A. (1996) Cation-pi interactions in chemistry and biology: a new view of benzene, Phe, Tyr, and Trp, *Science* 271, 163-168.
72. Cashin, A. L., Petersson, E. J., Lester, H. A., and Dougherty, D. A. (2005) Using physical chemistry to differentiate nicotinic from cholinergic agonists at the nicotinic acetylcholine receptor, *J Am Chem Soc* 127, 350-356.
73. Beene, D. L., Brandt, G. S., Zhong, W., Zacharias, N. M., Lester, H. A., and Dougherty, D. A. (2002) Cation-pi interactions in ligand recognition by serotonergic (5-HT_{3A}) and nicotinic acetylcholine receptors: the anomalous binding properties of nicotine, *Biochemistry* 41, 10262-10269.
74. Petersson, E. J., Brandt, G. S., Zacharias, N. M., Dougherty, D. A., and Lester, H. A. (2003) Caging proteins through unnatural amino acid mutagenesis, *Methods Enzymol* 360, 258-273.
75. Williams, K., Russell, S. L., Shen, Y. M., and Molinoff, P. B. (1993) Developmental switch in the expression of NMDA receptors occurs in vivo and in vitro, *Neuron* 10, 267-278.
76. Green, T., Rogers, C. A., Contractor, A., and Heinemann, S. F. (2002) NMDA receptors formed by NR1 in *Xenopus laevis* oocytes do not contain the endogenous subunit XenU1, *Mol Pharmacol* 61, 326-333.
77. Hille, B. (2001) *Ion channels of excitable membranes*, 3rd ed., Sinauer, Sunderland, Mass.
78. Lummis, S. C., D, L. B., Harrison, N. J., Lester, H. A., and Dougherty, D. A. (2005) A cation-pi binding interaction with a tyrosine in the binding site of the GABAC receptor, *Chem Biol* 12, 993-997.
79. Wollmuth, L. P., Kuner, T., and Sakmann, B. (1998) Intracellular Mg²⁺ interacts with structural determinants of the narrow constriction contributed by the NR1-subunit in the NMDA receptor channel, *J Physiol* 506 (Pt 1), 33-52.
80. Kuner, T., Seeburg, P. H., and Guy, H. R. (2003) A common architecture for K⁺ channels and ionotropic glutamate receptors?, *Trends Neurosci* 26, 27-32.
81. Doyle, D. A., Morais Cabral, J., Pfuetzner, R. A., Kuo, A., Gulbis, J. M., Cohen, S. L., Chait, B. T., and MacKinnon, R. (1998) The structure of the potassium channel: molecular basis of K⁺ conduction and selectivity, *Science* 280, 69-77.
82. Hargreaves, R. J., Hill, R. G., and Iversen, L. L. (1994) Neuroprotective NMDA antagonists: the controversy over their potential for adverse effects on cortical neuronal morphology, *Acta Neurochir Suppl (Wien)* 60, 15-19.
83. Frausto da Silva, J. J. R. a. W., R.J.P. (1991) *The Biological Chemistry of the Elements* Vol. 1, Clarendon Press, Oxford.
84. Falke, J. J., Drake, S. K., Hazard, A. L., and Peersen, O. B. (1994) Molecular tuning of ion binding to calcium signaling proteins, *Q Rev Biophys* 27, 219-290.

85. Torrice, M. M. (2008) Chemical-scale studies of the nicotinic and muscarinic acetylcholine receptors, in *Chemistry and Chemical Engineering*, California Institute of Technology, Pasadena.
86. Cashin, A. L., Torrice, M. M., McMenimen, K. A., Lester, H. A., and Dougherty, D. A. (2007) Chemical-scale studies on the role of a conserved aspartate in preorganizing the agonist binding site of the nicotinic acetylcholine receptor, *Biochemistry* 46, 630-639.
87. Cashin, A. L. (2006) Chemical scale investigations of drug-receptor interactions at the nicotinic acetylcholine receptor., in *Chemistry and Chemical Engineering*, California Institute of Technology, Pasadena.
88. Chen, H. S., Pellegrini, J. W., Aggarwal, S. K., Lei, S. Z., Warach, S., Jensen, F. E., and Lipton, S. A. (1992) Open-channel block of N-methyl-D-aspartate (NMDA) responses by memantine: therapeutic advantage against NMDA receptor-mediated neurotoxicity, *J Neurosci* 12, 4427-4436.
89. Chen, H. S., and Lipton, S. A. (1997) Mechanism of memantine block of NMDA-activated channels in rat retinal ganglion cells: uncompetitive antagonism, *J Physiol* 499 (Pt 1), 27-46.
90. Lipton, S. A., and Chen, H. S. (2005) Paradigm shift in NMDA receptor drug development, *Expert Opin Ther Targets* 9, 427-429.
91. Kashiwagi, K., Masuko, T., Nguyen, C. D., Kuno, T., Tanaka, I., Igarashi, K., and Williams, K. (2002) Channel blockers acting at N-methyl-D-aspartate receptors: differential effects of mutations in the vestibule and ion channel pore, *Mol Pharmacol* 61, 533-545.
92. Chen, H. S., and Lipton, S. A. (2005) Pharmacological implications of two distinct mechanisms of interaction of memantine with N-methyl-D-aspartate-gated channels, *J Pharmacol Exp Ther* 314, 961-971.
93. Sobolevsky, A. I., Koshelev, S. G., and Khodorov, B. I. (1998) Interaction of memantine and amantadine with agonist-unbound NMDA-receptor channels in acutely isolated rat hippocampal neurons, *J Physiol* 512 (Pt 1), 47-60.
94. Sobolevsky, A., and Koshelev, S. (1998) Two blocking sites of amino-adamantane derivatives in open N-methyl-D-aspartate channels, *Biophys J* 74, 1305-1319.
95. Bresink, I., Benke, T. A., Collett, V. J., Seal, A. J., Parsons, C. G., Henley, J. M., and Collingridge, G. L. (1996) Effects of memantine on recombinant rat NMDA receptors expressed in HEK 293 cells, *Br J Pharmacol* 119, 195-204.
96. Blanpied, T. A., Boeckman, F. A., Aizenman, E., and Johnson, J. W. (1997) Trapping channel block of NMDA-activated responses by amantadine and memantine, *J Neurophysiol* 77, 309-323.
97. Antonov, S. M., and Johnson, J. W. (1996) Voltage-dependent interaction of open-channel blocking molecules with gating of NMDA receptors in rat cortical neurons, *J Physiol* 493 (Pt 2), 425-445.
98. McMenimen, K. A., Dougherty, D. A., Lester, H. A., and Petersson, E. J. (2006) Probing the Mg²⁺ blockade site of an N-methyl-D-aspartate (NMDA) receptor with unnatural amino acid mutagenesis, *ACS Chem Biol* 1, 227-234.

99. Wrighton, D. C., Baker, E. J., Chen, P. E., and Wyllie, D. J. (2008) Mg²⁺ and memantine block of rat recombinant NMDA receptors containing chimeric NR2A/2D subunits expressed in *Xenopus laevis* oocytes, *J Physiol* 586, 211-225.
100. Nowak, M. W., Gallivan, J. P., Silverman, S. K., Labarca, C. G., Dougherty, D. A., and Lester, H. A. (1998) In vivo incorporation of unnatural amino acids into ion channels in *Xenopus* oocyte expression system, *Methods Enzymol* 293, 504-529.
101. Spier, A. D., and Lummis, S. C. (2000) The role of tryptophan residues in the 5-Hydroxytryptamine(3) receptor ligand binding domain, *J Biol Chem* 275, 5620-5625.
102. Lummis, S. C., Beene, D. L., Lee, L. W., Lester, H. A., Broadhurst, R. W., and Dougherty, D. A. (2005) Cis-trans isomerization at a proline opens the pore of a neurotransmitter-gated ion channel, *Nature* 438, 248-252.
103. Boys, S. F. a. B., F. (1970) *Molecular Physics*, 553-557.
104. Frisch, M. J. T., G. W.; Schlegel, H. B.; Scuseria, G. E.; Robb, M. A.; , Cheeseman, J. R. Z., V. G.; J. A. Montgomery, J.; Stratmann, R. E.; Burant, J. C.; Dapprich, S. M., J. M.; Daniels, A. D.; Kudin, K. N.; Strain, M. C.; Farkas, O.; , Tomasi, J. B., V.; Cossi, M.; Cammi, R.; Mennucci, B.; Pomelli, C.; Adamo, C.; , and Clifford, S. O., J.; Petersson, G. A.; Ayala, P. Y, et al. (1998) Frisch, M. J.; Trucks, G. W.; Schlegel, H. B.; Scuseria, G. E.; Robb, M. A.; Cheeseman, J. R.; Zakrzewski, V. G.; J. A. Montgomery, J.; Stratmann, R. E.; Burant, J. C.; Dapprich, S.; Millam, J. M.; Daniels, A. D.; Kudin, K. N.; Strain, M. C.; Farkas, O.; Tomasi, J.; Barone, V.; Cossi, M.; Cammi, R.; Mennucci, B.; Pomelli, C.; Adamo, C.; Clifford, S.; Ochterski, J.; Petersson, G. A.; Ayala, P. Y, in *Gaussian 98 Revision A.9 ed.*, Gaussian Incorporated, Pittsburgh, PA.